Manuscript Number: B30049R1

Title: Record of mega-earthquakes in subduction thrusts: the black fault rocks of Pasagshak Point (Kodiak Island, Alaska)

Short Title: Record of mega-earthquakes in subduction thrusts, Kodiak Island, Ak

Article Type: Article

Keywords: subduction thrust, seismogenic zone, cataclasite, pseudotachylyte, granular flow, Kodiak Accretionary Complex

Corresponding Author: Dr. Francesca Meneghini, Ph.D

Corresponding Author's Institution: University of Pisa

First Author: Francesca Meneghini, Ph.D

Order of Authors: Francesca Meneghini, Ph.D; Giulio Di Toro; Christen D Rowe; Casey J Moore; Akito Tsutsumi; Asuka Yamaguchi

Abstract: On Kodiak Island (Alaska), decimeter-thick black fault rocks (BFR) are at the core of 10's meters-thick foliated cataclasites. Cataclasites belong to mélanges regarded as paleo-décollement active at 12-14 km depth and 230-260oC. Each black layer is mappable for tens of meters along strike. The BFR feature a complex layering made at microscale by alternation of granular and crystalline microtextures, composed of micron-scale sub-rounded quartz and plagioclase in an ultrafine, phyllosilicate-rich matrix. In the crystalline microlayers, tabular zoned microlites of plagioclase make much of the matrix. No such feldspars are found in the cataclasite. We interpret crystalline microlayers as pseudotachylytes. The granular microlayers show higher grain size variability, crushed microlites and textures typical of fluidization and granular flow deformation. Crosscutting relationships between granular and crystalline microlayers include flow and intrusion structures and mutual brittle truncation. This suggests that each 10's centimeter-thick composite BFR record multiple pulses of seismic slip. In each pulse, ultracomminuted fluidized material and friction melt formed and deformed together in a ductile fashion. Brittle truncation by another pulse occurred after solidification of the friction melt and the fluidized rock.
XRPD and XRF analyses show that BFR have similar mineral composition and chemical content as the cataclasites. The observed systematic chemical differences cannot be explained by bulk or preferential melting of any of the cataclasite components. The presence of an open, fluid-infiltrated system with BFR later alteration is suggested. The geochemical results indicate that these subduction-related pseudotachylytes, differ from those typically described in crystalline rocks and other tectonic settings.

Suggested Reviewers:

Opposed Reviewers:

Response to Reviewers: We thank the associate editor and reviewers for their comments. The summary of salient points to be addressed made by the Associate Editor was particularly helpful for us to improve the manuscript quality. In an attached file we have listed point-by-point all the changes made according to what suggested by Associate Editor and reviewer Magloughlin. Responses are in italics, bold.

Since a lot of changes have been made, we are submitting as supplementary material a word file of the manuscript text with Track Changes. We hope this will show easier the changes made to the Associate Editor and reviewers.

To commit comment 128 by reviewer Magloughlin we have redrawn one figure (Fig.11 of new version) and we are now requesting Figure 11 to be printed in colors.

We hope the new submitted version of manuscript will satisfy reviewer's requests and Journal's standards.

Cover Letter

Click here to download Cover Letter: response to reviewers.doc

Record of mega-earthquakes in subduction thrusts: the black fault rocks of Pasagshak Point (Kodiak Island, Alaska)

Meneghini F.[1,5,*], Di Toro G.[2,3], Rowe C.D.[4], Moore J.C.[5], Tsutsumi A.[6], Yamaguchi A.[7]

[1] Dipartimento di Scienze della Terra, Università di Pisa, via S. Maria, 53, 56126 Pisa, Italy
[2] Dipartimento di Geoscienze, Università di Padova, Via Giotto 1, 35137 Padova, Italy
[3] Istituto Nazionale di Geofisica e Vulcanologia, Via di Vigna Murata 605, Roma, Italy
[4] Department of Geological Sciences, University of Cape Town, University Avenue, Rondebosch 7701, South Africa
[5] Earth and Planetary Sciences Department, University of California at Santa Cruz, Santa Cruz, CA 95064, U.S.A.
[6] Department of Geology & Mineralogy, Division of Earth & Planetary Sciences, Kyoto University, Kitashirakawa Oiwakecho, Sakyo-ku, Kyoto, 606-8502, Japan
[7] Department of Earth and Planetary Science, The University of Tokyo, 7-3-1 Hongo, Bunkyo-ku, Tokyo, 113-0033, Japan

Keywords: subduction thrust, seismogenic zone, cataclasite, pseudotachylyte, granular flow, Kodiak Accretionary Complex

[*] corresponding author

ABSTRACT

On Kodiak Island (Alaska), decimeter-thick black fault rocks (BFR) are at the core of 10's meters-thick foliated cataclasites. The cataclasites belong to mélange zones regarded as paleo-décollement active at 12-14 km depth and 230-260^{o}C. Each black layer is mappable for tens of meters along strike.

The BFR feature a complex layering made at microscale by alternation of granular and crystalline microtextures, both composed of micron-scale sub-rounded quartz and plagioclase in an ultrafine, phyllosilicate-rich matrix. In the crystalline microlayers, tabular zoned microlites of plagioclase make much of the matrix. No such feldspars have been found in the cataclasite. We interpret these crystalline microlayers as pseudotachylytes. The granular microlayers show higher grain size variability, crushed microlites and textures typical of fluidization and granular flow deformation. Crosscutting relationships between granular and crystalline microlayers include flow and intrusion structures and mutual brittle truncation. This suggests that each 10's centimeter-thick composite BFR record multiple pulses of seismic slip. In each pulse, ultracomminuted fluidized material and friction melt formed and deformed together in a ductile fashion. Brittle truncation by another pulse occurred after solidification of the friction melt and the fluidized rock.

XRPD and XRF analyses show that BFR have similar mineral composition and chemical content as the cataclasites. The observed systematic chemical differences cannot be explained by bulk or preferential melting of any of the cataclasite components. The presence of an open, fluid-infiltrated system with BFR later alteration is suggested. The geochemical results indicate that these subduction-related pseudotachylytes, differ from those typically described in crystalline rocks and other tectonic settings.

1. INTRODUCTION

Theoretical work (Rice, 2006), and seismological observations (e.g., Ide and Takeo, 1997) suggest that earthquakes occur because fault strength decreases with increasing slip or slip rate. Several coseismic fault-weakening mechanisms have been proposed in the literature (for a review see Wibberley et al., 2008). At present, however, most mechanisms, with the exception of frictional melt lubrication, have been described from a theoretical and experimental point of view, without clearly identifying their possible geological expression in the fault rock record. Particularly, only tectonic pseudotachylytes (solidified friction-induced melts produced during seismic slip) are so far unambiguously recognized as the signature of ancient earthquakes (Sibson, 1975; Cowan, 1999).

Despite the intense seismic activity and the occurrence of the largest earthquakes in subduction zones, evidence for pseudotachylytes is not widespread in this tectonic setting (Ikesawa et al., 2003; Kitamura et al., 2005; Rowe et al., 2005; Sibson and Toy, 2006; Ujiie et al., 2007; 2009). Why are pseudotachylytes so rare along subduction mega-thrusts, and which other fault rocks (e.g., fludized cataclasites, Lin, 1996; Monzawa et al., 2003; Otsuki et al, 2003; Ujiie et al., 2007), if any, do record seismic ruptures? Understanding of the seismic cycle, including the transition from aseismic to seismic slip and the activation of fault weakening mechanisms along subduction mega-thrusts, depends on (1) recognizing and discriminating rocks produced during seismic slip and (2) understanding the factors that control their production. Because drilling of active faults has yet to penetrate the seismogenic zone of subduction thrusts, the investigation of fault zones exhumed at the Earth's surface provide valuable information on fault processes responsible for seismogenic behavior.

Here we report on a décollement-system thrust fault preserved in an accreted mélange unit of the Kodiak accretionary complex, representing the fossil analogue of the active Alaskan subduction, a similar setting to the locus of the 1964 M_w9.2 Alaskan earthquake. We studied a steeply-dipping, strike-parallel cross section extending approximately 3.5 km along the coast of the southern Pasagshak Peninsula (Fig. 1). Faulting occurred at 12–14 km depth and 230–260°C (e.g. Vrolijk et al., 1988), below the upper aseismic to seismic transition, within the seismogenic zone (e.g., Bilek and Lay, 1999). Previously, we reported on the occurrence of a massive, black, ultra-fine-grained fault rock associated with foliated cataclasites and that black fault rocks contained pseudotachylyte (Rowe et al., 2005). Here we describe detailed microstructural, mineralogical and geochemical analyses of the black fault rocks, performed after additional fieldwork and sampling. Specifically, the use of the Field Emission Scanning Electron Microscopy (FE-SEM), allowed a better definition of the microstructure and composition of the black fault rocks (hereafter BFR) and interpretation of these rocks as recording complex events of seismic slip that locally resulted in frictional melting. The microtextural evidence unequivocally confirm an origin by friction melting, but the geochemical data suggest peculiarity in the BFR versus apparent source rock compositions when compared with what are generally reported patterns in pseudotachylytes from different tectonic settings. Most described pseudotachylytes are hosted in the continental crust and in collisional settings (e.g., among others, Magloughlin and

Spray, 1992; Maddock, 1992; Snoke, Tullis and Todd, 1998; Di Toro and Pennacchioni, 2004; Lin, 2008; Di Toro et al., 2009 and reference therein).

2. GEOLOGIC SETTING AND STUDY AREA

The Kodiak Accretionary Complex of SE Alaska (Fig. 1) exposes a tectonic stack of units that were underthrust and accreted from Jurassic to Eocene (Moore, 1969; Moore and Allwardt, 1980; Byrne, 1982; Fisher and Byrne, 1987; Sample and Moore, 1987; Roeske et al., 1989). The complex has modern analogues offshore, in the Eastern Aleutian Trench (Plafker et al., 1994). The units, made up of oceanic igneous and sedimentary rocks, have a mean NE-SW structural strike, decreasing in age and metamorphic grade toward the SE (Fig. 1). Each terrane is representative of an episode of subduction and accretion (Sample and Reid, 2003); those classified as mélanges have been previously interpreted as paleo-décollement zones (Byrne, 1984; Vrolijk et al., 1988).

Almost the 70% of the area of Kodiak Island is occupied by the Kodiak and Ghost Rocks formations, representing periods of voluminous sediment accretion that occurred in a relatively short time span: 10-13 Ma for the Kodiak Formation and less than 5 Ma for the Ghost Rocks Formation (Fisher and Byrne, 1987).

2.1 Ghost Rocks Formation and the section of Pasagshak Point

The structural base of the Ghost Rocks Formation crops out along the Pasagshak Point peninsula (Fig. 1). The Ghost Rocks Formation is a mélange section with a structural thickness of 5 to 10 km, whose original sedimentary sequence (turbiditic deposits and volcanic rocks) is interpreted as deposited above the Pacific or Resurrection plate oceanic crust, from latest Cretaceous to early Paleocene (Byrne, 1984; Hausseler et al. 2003). The Ghost Rocks Formation is over thrust by the Kodiak Formation, while its structural base is a thrust fault placing the Ghost Rocks over Eocene sedimentary units (Fig. 1).

Although displaying a highly variable structural style and degree of disruption, the Ghost Rocks Formation can be described overall as a mélange, made of blocks of coherent, thinly-bedded turbidite and massive sandstone separated by variably sheared and disrupted dark gray to black shale. Minor amounts of pillow basalt and hyaloclastite also occur (Byrne, 1984). In the less deformed sections, sedimentary structures confirm the trench-turbidite origin of the sedimentary sequence (Byrne, 1984). Maximum burial temperature of the basal Ghost Rocks mélange is estimated at 230-260°C from fluid inclusions studies (Vrolijk et al., 1988), mean vitrinite reflectance (250 ± 10°C, Rowe, 2007), and the occurrence of syntectonic prehnite and pumpellyite.

In general, mélange zones increase in frequency, degree of stratal disruption, and intensity of shear deformation toward the southeast, i.e. toward the structural base of the formation. The structural and deformational evolution of this mélange terrane was deciphered by Byrne (1984) and Fisher and Byrne (1987), who attributed the mélange formation to high shear strain and dewatering of a sediment pile undergoing progressive underthrusting along a paleo-décollement zone.

In the 2004 and 2006 field seasons, we mapped the structural base of the Ghost Rock Formation along the Pagashak Point coast with meter scale resolution and, on GPS located, well-exposed outcrops, structural analyses were performed at a centimeter scale (Figs. 1, 2). All the rock types found in the Ghost Rocks Formation are present along the measured section as variably sized blocks (from mm to tens of meters) of massive sandstone, thinly bedded turbiditic sections and, rarely, pillow basalt, in a pelitic dark gray matrix. The fabrics in each rock type record a deformation history spanning from burial to accretion through compaction and dewatering, stratal disruption and shearing (Byrne, 1984; Fisher and Byrne, 1987; Sample and Moore, 1987). The structural fabrics are consistent with NW-dipping, slightly left oblique, subduction at the time of mélange formation (Rowe et al., 2005; Rowe, 2007). Other than distributed web structures in sandstone, the earliest deformation fabrics are boudinage and calcite- and quartz-filled extension veins oriented at a high angle to the bedding, suggesting layer-parallel extension, responsible for the disruption of the sedimentary sequence. A subsequent event of shear-related bedding-parallel shortening is recorded in the coherent blocks in the form of irregular, complex tight to sub-isoclinal folds. In the pelitic sections, the typical deformation fabric is a pervasive, penetrative scaly cleavage, associated with pressure solution, and commonly parallel to the axial plane of the folds.

2.2 Shear localization within the mélange: the cataclasite zones

Localization of shear strain in the Ghost Rock mélange is recorded by four sub-parallel high-strain cataclasite zones mapped within a structural thickness of less than 1 km (Figs. 1, 2). Cataclasite strands are up to 40 m thick, but typically 15-20 m thick, and can be followed continuously along strike for distances of about 2.5 km. The cataclasite features centimeter to decimeter sized sandstone fragments enclosed in very fine-grained reddish to brown pelitic matrix, with rare ribbons of greenstone. Cataclasite meso-structures range between three end-member types, identified on the basis of clast concentration and strength/style of foliation (Fig. 3): (1) clast-rich or (2) matrix-supported foliated cataclasites (sub-rounded to angular sandstone clasts and boudins immersed in scaly foliated highly sheared matrix, Fig. 3A), and (3) non-foliated cataclasites (matrix-supported, with rounded grains of various size in an apparently non-foliated matrix, Fig. 3B). Cataclasite domains dominated by one type of texture can be bounded by thin shear surfaces or may have gradational transitions to another type. They may reflect strain and strain rate partitioning during shearing. The boundaries of the cataclasite zones with the hosting Ghost Rocks mélange also vary from sharp, possibly fault contacts, to gradational transitions.

3. BLACK FAULT ROCKS (BFR): FIELD DESCRIPTION

Three distinct layers of ultra-fine-grained black fault rocks (BFR) were mapped as bands sharply crosscutting or intruding three of the cataclastic shear zones (Figs. 1, 2, 4). Each BFR layer can be traced continuously up to tens of meters along a single outcrop (Fig. 4A), and structural correlations can be made across ca. 2.5 km of section: going from southwest to northeast a single layer can be correlated from GPS points WPT015, through WPT014 and WPT009, to BLKSTF (Fig. 1). At all these localities the BFR unit occurs at the contact between cataclasite and mélange: the same layer has been observed along this contact at a number of localities in between. These intermediate localities were not studied in detail because they are either difficult to access or poorly exposed. Nevertheless they allow confident long distance correlation.

Of the three, the uppermost and lowermost BFR layers occur within each cataclasite zone, cutting the cataclasite fabric at a low angle (Figs. 2, 4B). The middle BFR layer is located at the interface between an underlying cataclasite zone and an upper unit of massive sandstone of the mélange (Figs. 2, 4A).

BFR horizons range from less than 10 cm to more than 30 cm in thickness, and are characterized by alternation of layers showing two end-members textures (Figs. 4 and 5A):

- Aphanitic BFR layers

Aphanitic BFR rocks are harder than surrounding rocks and show satin, chert-like luster (Fig. 4C). They are gray-black to blue-black, with local concoidal fracture and no foliation. Aphanitic layers are often subtly stratified: individual sub-layers are up to 2 cm thick and show distinctive, layer-orthogonal jointing. No grains are visible in hand sample, except for some chalcopyrite crystals scattered along sub-layer contacts and at the contact with the host cataclasite.

- Grain-supported BFR layers

Grain-supported layers are made of very fine angular grains (up to 1 mm), the largest of which show the same satin luster as aphanitic layers on weathered surfaces (Fig. 4D). The matrix is not easily resolvable but is dominantly composed of finer grains of the same aphanitic material. The matrix locally shows a weak, anastomosing cleavage comparable with that of cataclasite and with mean orientation making a low angle to that of the host cataclasite fabric. Black granular layers occur both singly and in association with black aphanitic layers.

Grain-supported and aphanitic layers are complexly inter-layered to form the thick typically banded aspect of BFR at field scale (Figs. 4A, 5A). The outcrop named WPT015 (Fig. 1) features the thickest BFR composite unit of the investigated area, ranging between 7.5 cm to 32 cm. The composite unit is made up of individual cm-scale bands of aphanitic and grain-supported BFR layers, but the entire thickness is divided by a sharp contact into two sub-units, each one characterized by coherent folding and deformation of the banded layers. This observation suggests that each coherently folded, composite sub-unit was deforming in a ductile fashion before being brittlely truncated by the second sub-layer.

3.1 Cataclasite-BFR boundary: flow and intrusion structures

The basal contact of the BFR with cataclasites is commonly sharp and sub-planar (Fig. 5A). In contrast, the upper contact is often characterized by injections and flow structures, whose morphology seems to be controlled by the lithology of the hangingwall rock (Brodsky et al 2009). When the upper contact is with massive sandstone bodies, BFR locally develop injection veins similar to those reported in pseudotachylyte-bearing faults in other settings (e.g. Sibson, 1975; Magloughlin and Spray, 1992; Snoke et al., 1998; Di Toro et al., 2005). Injections are wedge-shaped with sharp, semi-planar walls (Fig. 5B). In contrast, when the upper contact is made of cataclasites, the BFR develop intrusion structures with variable morphology (Fig. 5C), resembling flow structures in volcanic rocks (see McPhie et al., 1993), or flame structures typical of sedimentary rocks (Brodsky et al., 2009). Around the intrusion, the cataclasite fabric is deformed by granular-ductile flow (folding, Fig. 5C, Brodsky et al., 2009). Both upper and lower cataclasite-BFR structural boundaries also feature scattered, altered sulfides in trails or patches.

4. MICROSTRUCTURES OF THE FAULT ROCKS

The host cataclasites and the black fault rocks were studied using optical and high resolution Field Emission SEM microscopy. The main goal was to investigate the difference in texture and structure and the mutual relationships between the two fault rocks, in order to determine their mechanisms of formation.

Microstructural investigations were conducted with a scanning electron microscope (SEM) Camscan-Mx2500 (resolution in back-scattering mode of 100 nm), equipped with EDS microanalysis (Dipartimento di Geoscienze, University of Padova), and with a high-resolution Field Emission SEM (FE-SEM JEOL 7000, with resolution in back-scattering mode of 4 nm, hosted at the Istituto Nazionale di Geofisica e Vulcanologia, Rome, Italy.

A contrast in grain size and grain shape clearly differentiates the cataclasites from BFR. In addition, micro-scale structure with high-resolution microscopy revealed two distinct classes within the BFR, which could not be clearly differentiated optically. A comparison between these classes with those identified in the field was also made.

4.1 BFR microstructures

Under the optical microscope, the BFR microstructure (Fig. 6A) is defined by bright, sub-rounded quartz grains (long axis up to 1 mm, on average, about 0.1 mm), in an irresolvable greenish matrix. As seen in the field, a boundary-parallel banding (Figs. 6A, B) is a common feature in BFR samples, with each layer distinguished by: color, distribution of larger clasts and occurrence of re-worked grains, abundance of phyllosilicates, and the strength of pressure solution fabrics. Phyllosilicate-rich (chlorite and clay minerals) greenish layers with very fine grain size (BFR-cx in Fig. 6A) alternate with light green horizons, with a more granular aspect due to a concentration of quartz grains (BFR-gr in Fig. 6A).

Back Scatter Electron (BSE) SEM and, in particular, high-resolution studies of the microstructure of BFRs also revealed two types of microtextures (Figs.6B to 6F), that complexly alternate. The bulk texture at this scale is a fine-grained assemblage of rounded to sub-rounded grains of quartz and less abundant feldspars, with grain long axis up to 10 μm, floating in a very fine-grained matrix (diameter of grains up to 4 μm) of a tightly-packed assemblage of quartz, feldspars, chlorite and illite. However, the shape, mineralogy, and structure of grains and matrix require definition of two distinct microtextures, referred to as **granular (BFR-gr)** and **crystalline (BFR-cx)** BFRs. Detailed selective sampling and analyses of the layers identified in the field show that while the field-defined grain-supported BFR only show granular microtexture, the aphanitic BFR show, at microscale, a complex alternation of microlayers featuring granular and crystalline microtextures, that resemble the style of layering seen on field scale. Only aphanitic layers contain crystalline microlayers.

The **crystalline microlayers** seen in FE-SEM imagery ("BFR-cx" in Fig. 6) contain grains of subrounded quartz and euhedral feldspars grains (1 to 2 μm in length), with interstitial, randomly oriented, platy chlorite (light gray, whitish) and less abundant illite (medium gray), both 1 μm in length (Fig. 7A). Most plagioclase grains in these layers are idiomorphic, with tabular shape, and they show various types of zoning (Lofgren, 1980 for a review about zoning in feldspars): (1) some plagioclase crystals show normal zoning with Ca-rich, bright core and Na-rich darker rims; (2) some show reverse zoning, with Na-rich core and Ca-rich rims, and, (3) some others are characterized by repeated, < 0.1 μm-thick alternation from Ca-rich- to Na-rich zones, going from the core to the rim (Fig. 6D). Other feldspars are fractured (across zoning), whereas some nucleated in interstitial space (zoning follows the external shape), or, locally, bear irregular boundaries similar to resorption features (Fig. 6D). Quartz grains are also locally embayed, with phyllosilicates arranged at their margins (Fig. 6E).

In contrast, the **granular microlayers** are dark grey, and have a tightly packed matrix of sub-rounded quartz and feldspars grains ("BFR-gr" in Fig. 6), with grain size variable from 3 μm to less than 1 μm. Smaller, sub-μm grains of quartz and feldspar fill the interstices together with μm to sub-μm chlorite and illite grains (Fig. 7B). The decrease in phyllosilicate abundance and grain size is dramatic, compared to the crystalline microlayers (Fig. 7B). Feldspars are locally euhedral and zoned, but an increase in the occurrence of crushed feldspars is observed in the granular microlayers (Figs. 6C, F).

Both microlayers commonly contain sub-spherical grains (<1 μm) of Ti-oxides and sulfides (Fe-sulfides and chalcopyrite) and small framboidal pyrite. Although commonly scatterely across layers (Figs. 6, 7), trails of oxides and sulfides have been previously reported in the BFR (Rowe et al., 2005, Figure 3). Rowe et al. (2005, page 938 and Figure 3) also stressed the rarity or absence of such minerals in the hosting cataclasite. As previously mentioned in this paper, chalcopyrite also tends to concentrate at BFR sublayers boundaries, similar to reported observations of pseudotachylyte veins from the Nason Terrane (Magloughlin, 1989, Figure 5a; 1992; 2005).

Pressure solution is ubiquitous in both BFR and in the host cataclasite, as suggested by the presence of a sinuous arrangement of black thin seams sub-parallel to BFR boundary and to the foliation in the cataclasites (Fig. 6A). Generally, pressure solution tends to concentrate in granular microlayers, where seams anastomose around grains. A similar pattern of pressure solution has been described in pseudotachylyte veins from the Nason Terrane of Northern Cascades (Magloughlin, 1989, fig. 5c)

Mutual crosscutting relationships occur between the two layers. Reworked clasts of crystalline microlayers are found in the granular microlayers (Fig. 8A) and reworked clasts of granular microlayers are found in crystalline microlayers (Fig. 8B). Along the planar boundaries between layers we observe clasts from microcrystalline layers indenting into granular microlayers (Fig. 6B), as well as tabular feldspars of crystalline microlayers sharply truncated by granular microlayers (Fig. 8C). Flow deformation incorporates both types of BFR layers as sheath fold-like structures, dragging of bigger clasts, flow banding and entrainment structures (Fig. 8D; see also Fig. 3 of Rowe et al., 2005) recalling "mixing" of immiscible fluids, or the flow banding commonly seen in volcanic rocks (Phillpotts, 1982; McPhie et al., 1993 and references therein). These microstructures resemble the outcrop-scale entrainment structures of BFR into cataclasites (Fig. 5C), and have been extensively described in pseudotachylytes (among many others: Magloughlin 1989; 1992; 2005; Craddock and Magloughlin, 2005).

As observed at outcrop-scale, injection veins are uncommon and occur only when BFR are in contact with sandstone units from mélange, at the boundaries of the cataclasite units (Fig. 8E).

To summarize, main differences between the BFR crystalline and granular microlayers are (Figs. 6, 7):

- the matrix of the crystalline microlayers shows a more bimodal grain size distribution than the granular microlayers, with similar maximum grain size (2-3 μm) but larger minimum grain size (1 μm vs. sub-μm, respectively, Fig.7)
- packing of feldspars in the matrix is less dense in the crystalline microlayers, where they are coated with chlorite and illite, so that they are not in contact, and there are few matrix grains of feldspar (Fig.7),
- by comparing BSE high resolution images, chlorite constitutes up to the 20% of crystalline microlayers, but only less than 10% in the granular microlayers (Figs. 6, 7),
- tabular, complexly zoned plagioclases are observed in both layers, but they occur preferentially in the crystalline microlayers, and are commonly fractured when found in the granular microlayers (compare Figs. 6D and 6F, 7),
- clasts of crystalline microlayers occur in granular microlayers and vice versa.

4.2 Cataclasite microstructures

Most of the cataclasite hosting the BFR are of foliated-type, therefore only foliated samples are described here. Foliated cataclasite microstructures comprise rotated, elongated angular to rounded clasts of sandstones, quartz and subordinate plagioclase suspended in a phyllosilicate-rich matrix (Fig. 9A). Clast size varies from few millimeters down to the sub-millimeter-scale. The matrix is characterized by a penetrative cleavage defined by the shape preferred orientation of chlorite and illite minerals, wrapping around big clasts. Locally, strain fringes at *boudin* edges, and fragment of calcite veins in sandstone and quartz clasts, also occur.

The above microstructures suggest that cataclastic flow and pressure solution are the main deformation mechanisms.

We also used the high resolution FE-SEM to investigate the microstructures of the cataclasites (Fig. 9B). At the FE-SEM scale, cataclasites are made up of angular to subrounded quartz and subordinate feldspar clasts up to 10-20 μm long, embedded in a fine matrix of about 1 μm-size feldspar, quartz, chlorite, illite, plus minor titanite and euhedral apatite.

Direct measurements of porosity indicate a cataclasite porosity of 5% and a BFR porosity of 1.5% (Brodsky et al. 2009, compare Figs. 6B and 6C with 9B).

Summarizing, the contrasts between the BFR and the cataclasites microstructures are:

i) quartz and plagioclase clasts in all BFR layers are sub-rounded, whereas in the cataclasites they are angular.

ii) plagioclase in the crystalline microlayers of BFR are euhedral and zoned. No idiomorphic, tabular or zoned plagioclase have been identified in the cataclasites.

iii) phyllosilicates in BFR crystalline microlayers are arranged between the feldspar grains, so that no preferred orientation of platy minerals is visible at any scale, except when flow structures occur. On the contrary, cataclasites show a strong preferred orientation of chlorite and illite flakes (compare Figs. 6C and 9B).

iv) grainsize in BFR is up to one order of magnitude finer than that of the cataclasites (compare Figs. 6C and 9B).

5. GEOCHEMISTRY AND MINERALOGY OF BFR AND CATACLASITES

The comparison of the mineralogical and geochemical analyses of BFR and cataclasite is crucial for deciphering the origin and formation processes of the BFR. To accomplish this goal, we collected oriented samples using a coring drill, at each selected locality, through transects across the BFR from the cataclasite of the footwall to the cataclasite or sandstone of the hanging wall (for an example of a sampling transect in a selected locality see Fig. 10A). XRPD and XRF analyses were performed to characterize the mineralogy, modal content and geochemistry of BFR and cataclasites. Results are summarized in Figures 10, 11 and in Tables 1 and 2.

5.1 Geochemistry

Wavelength Dispersive X-ray Fluorescence analyses were performed with a WDS Philips PW2400 equipped with Rhodium tube (Dipartimento di Geoscienze, Univ. of Padova). For analysis, powder samples were mixed and diluted at 1:10 with $Li_2B_4O_7$ and $LiBO_2$ flux and melted into glass beads. Loss on Ignition (LOI) was determined from weight lost after ignition at 860 °C for 20 minutes and at 980 °C for two hours. FeO was determined with permanganometry using a Rhodium tube. International rock standards were used for calibration.

The XRF data of BFR and associated cataclasites of each selected outcrop are displayed in Table 1, and the average cataclasites and BFR compositions with their standard deviation are reported in Table 2. For each transect (see example in Fig. 10A) the bulk composition of BFR was normalized versus the average cataclasites and is reported in Fig. 10B.

Cataclasite composition is uniform across the ~3.5 km along strike section measured (see Table 2, with minor variaiton in FeO, Fe_2O_3 and Ba). In contrast, BFR samples show a less uniform composition along the section. Systematic chemical differences are observed when comparing BFR to the associated cataclasite layers in each transect (Table 1 and Fig. 10), as well as the average BFR and cataclasite compositions (Table 2). For major elements (Table 1 and Fig. 10), we observe a significant increase in Na_2O, which is 67% to up to 150% higher in the BFR than in the cataclasites (except for one sample at WPTBLKSTF only showing a 34% increase). K_2O is systematically lower in BFR than in cataclasite, with a decrease ranging from 34% to 84%. LOI is also generally lower in the BFR, and CaO has no systematic relationship with the cataclasites. BFR samples contain remarkably higher Sr compared to the cataclasite, ranging between 160 and 212 %, and lower Rb (35 to 85% lower in BFR than in cataclasite). The same variations are recognized when looking at the mean compositions (Table 2). Here again we report higher Na_2O and Sr content, and a decrease in K_2O. Peculiar variations are shown in the transect at outcrop WPT009, where the BFR hangingwall sandstone. Here, Sr content in the BFR show a huge peak at 600% higher that in the cataclasite (see Tables 1 and 2). Similarly, this is the only transect where a clear CaO increase is observed in the BFR compared to the cataclasite (82%).

5.2 Mineralogy

X-ray powder diffraction data were obtained by continuous scanning with an automated diffractometer system equipped with a curved graphite diffracted-beam monochromator.

Analyses were performed with a Philips X'Change diffractometer (Dipartimento di Geoscienze, Univ. of Padova), using a long fine focus Cu X-ray tube operating at 40 kV and 30 mA. Diffraction profiles were obtained using a step interval of 0.02° 2θ with a counting time of 1 s. The scans were performed over the range 2-70° 2θ.

The XRPD data for BFR and associated cataclasites for each transect are reported in Fig.11. The mineralogy is consistent along the ca. 3.5 km of section analyzed, for both BFR and cataclasite. BFR and cataclasite have similar mineralogy. According to the chemical data, cataclasite mineralogy across the mapped section is more uniform than that of BFR. The most common minerals are quartz, plagioclase (albite), chlorite and illite. Plagioclase with a Ca-rich component phase was found only in three BFR samples. The diffraction patterns suggest an increase in plagioclase content in the BFR, associated with a slight decrease in chlorite and other phyllosilicates compared with the cataclasites (Fig. 11A).

The layering of granular and crystalline microtextures in BFR is extremely thin (mm- to μm-scale) and the above analyses describe the bulk compositions of BFR. Where layer separation was possible, analyses showed that the crystalline microlayer has a mineral composition similar to that of the bulk BFR, whereas the granular microlayer approaches the mineral composition of the cataclasites (Fig. 11B).

6. DISCUSSION

Pasagshak Point cataclasites are derived from the mélange and their major element chemistry is similar to that of the turbidites in the mélange. The main constituents of both lithotypes are quartz, albitic plagioclase, chlorite, and illite, consistent with the prehnite-pumpellyite facies conditions estimated for these rocks (Rowe, 2007).

The BFR are always associated with cataclasites, in crosscutting and intrusive relationships. Kinematic indicators found in the BFR are consistent with those of the cataclasite and mélange and BFR occurrence as reworked clasts in the cataclasites is also common (Fig. 3B). These relationships show that BFR evolved during and after the development of the cataclasites. In addition to being intimately spatially and structurally associated, BFR and cataclasite share the same mineralogy and some systematic geochemical variations. Therefore, we deduce that the

BFR originated from the cataclasite.

As discussed in the following sections, the texture and petrography of the BFR and their structural relationship with the cataclasite suggest frictional melting as a possible mechanism for the formation of at least the crystalline microlayers of the BFR, at the expense of the cataclasite (section 6.1). However, the BFR differ from most pseudotachylytes in that the bulk composition of the BFR vs. the hosting cataclasite is peculiar when compared to most other pseudotachylytes' relationship to their host/source rocks (section 6.4).

6.1 The BFR crystalline microlayers as pseudotachylytes

Comminution cannot explain the tabular morphology of the feldspar grains and the enrichment in feldspar and decrease in phyllosilicate content of the BFR with respect to cataclasites (Figs. 6, 10, 11). Our preliminary work included the interpretation of the BFR as containing pseudotachylytes (Rowe et al., 2005, figure 3), based on the identification of amygdules, embayed grains, and trails of Ti-oxides and sulfides. The high-resolution microstructural observations of the BFR reported here reveal a microporphyritic texture characterized by the widespread occurrence of zoned tabular feldspars, commonly making up more than the 50% of the BFR crystalline microlayers matrix. These micron-scale tabular plagioclases are the only zoned plagioclase found in any rocks in the study area. Therefore we interpret these feldspars as microlites crystallized from a melt, based on their euhedral shape and their zoning. The presence of microlites, together with the occurrence of embayed grains, vesicles and amygdules (Rowe et al., 2005), Ti-oxides and Fe-sulfides, suggest crystallization from a frictional melt (e.g., for a review of microstructures suggesting the melt origin of a fault rock, see Magloughlin and Spray, 1992; Di Toro et al., 2009) to produce the crystalline microlayers of the aphanitic BFR.

Frictional melting is a non-equilibrium process, so that selective melting of single minerals contributes to the production of the melt (Bowden and Tabor, 1950). In the case of frictional melting of geological materials, it has been observed that hydrous minerals with low individual melting point, such as amphibole and phyllosilicates, tend to contribute preferentially to the melt phase (Magloughlin and Spray, 1992). Other than melting point, a dependence of friction melting on the mechanical behavior of these minerals at high strain rates has been postulated, with properties like shear yield strengths, fracture toughnesses and thermal conductivities playing a special role (Shand, 1916; Spray, 1992). Therefore, the pseudotachylyte matrix is generally dominated by the glassy or crystalline equivalents of these hydrous phases, whereas quartz, feldspar and accessory refractory minerals generally survive as clasts (Shand, 1916; Philpotts and Miller, 1963; Allen 1979; Maddock 1986; 1992; Spray, 1987; 1992; Magloughlin; 1992; Magloughlin and Spray, 1992; Lin, 2008; Di Toro et al., 2009 and references therein). Following this general behavior, the production of Pasagshak Point microcrystalline layers by friction melting of cataclasites, would be predicted to occur with the low melting point chlorite and illite being the most susceptible to melting. However, the occurrence of plagioclase microlites in those layers, and their absence in any other rock of the study area, implies that feldspar must have also been a significant component of the melted grains. This implies that either the release of OH^- from hydrous phases caused depression of the feldspar melting point, (e.g. Spray, 1992), or that viscous shear heating increased the temperature of the melt above ~ 1100°C (Nielsen et al., 2008). Once melt cooling initiated, then, temperature conditions must have been favorable for crystallization of the microlites (section 6.4).

The very detailed imaging of microlites through FE-SEM allows us to comment on how they formed and on the characteristics of the friction melt.

Microlite nucleation, growth and zoning are controlled by the cooling history of the crystalline BFR microlayers. If we consider only the heat losses by diffusion, the temperature T after time t, at a distance x from the vein center of a melt layer hosted in a solid with an initial (ambient) temperature T_{hr}, is (Carslaw and Jaeger, 1959, p. 54; Jaeger, 1968):

$$T(x,t) = \frac{1}{2}T_0\left\{erf\left[\frac{a+x}{2\sqrt{\kappa\, t}}\right] + erf\left[\frac{a-x}{2\sqrt{\kappa\, t}}\right]\right\} + T_{hr} \qquad \text{Eq. 1}$$

where *erf* is the error function, $2a$ the layer thickness, T_o the initial layer temperature exceeding T_{hr} , and κ thermal diffusivity.

Fig. 12 shows the temperature evolution (Eq. 1) at the vein center for melt layers with an initial temperature of 1100^{o}C, an ambient temperature of 250^{o}C and a thickness of 1, 6 and 8 cm, respectively. This cooling model is very simple compared to the complexity observed in the composite BFR layers, for two main reasons: (1) we assumed the entire vein thickness is at the same initial temperature (1100^{o}C) when it starts to cool; (2) the temperature distribution at the initiation of cooling might be not homogenous. However the model is helpful to give us a general idea of the evolution of the crystalline, melt-bearing microlayers. We considered time durations of 4000s, as the crystallization window for albite-rich plagioclase is between 1000-800^{o}C for under-cooled systems, as is the case for centimeter-thick melt layers (Lesher et al., 1999; see Di Toro and Pennacchioni 2004 for a discussion). Typically, tectonic pseudotachylytes are less than 1-cm thick (Sibson, 1975; Di Toro et al., 2005) and plagioclase microlites are acicular, bow tie or dendritic, and un-zoned or normally zoned (Maddock 1983; Di Toro and Pennacchioni 2004, Lin, 2008). For such thin melt layers, cooling to ambient conditions (about 250^{o}C) is rapid (Fig. 12). Constant cooling rate and isothermal cooling steps experiments have shown that crystal morphology is affected by melt cooling rate, with tabular microlites crystallizing for slow cooling rates and acicular or bow-tie for rapid cooling rates (Lofgren, 1974; 1980; Corrigan, 1982). Though formed under similar ambient temperatures of about 250^{o}C, the slower cooling (Fig. 12) of the exceptionally thick Pasagshak Point pseudotachylytes might explain the tabular shape of the microlites and their ultrafine oscillatory to reverse zoning. Crystal morphology is the result of several parameters (e.g., superheating and under-cooling of the melt, presence and abundance of nuclei for crystallization, composition of the melts and fluids, oxygen fugacity), which interact by means of complex feedbacks (Lofgren, 1980). However, a rough approximation (tabular morphology = slow cooling, acicular morphology = fast cooling) suggests that the tabular morphology of plagioclase microlites is consistent with the exceptional thickness (and slow cooling rate) of the Pasagshak Point pseudotachylytes as compared to the other pseudotachylytes described in the literature. Zoning is preserved due to the extremely low diffusion rates of Na and Ca in the microlite lattice even at the sub-micron scale (see Smith and Brown, 1988 for a general review). However, the fact that the ultrafine zoning (reverse and oscillatory) was preserved and not homogenized, suggest that cooling rate was fast enough to further impede the diffusion of Na and Ca at the nanometer scale.

6.2 The BFR granular microlayers as comminuted fluidized gouge

Frictional melting during seismic slip is preceded by and contemporaneous (Spray 1995) with comminution and clast size reduction through pulverization at the rupture tip (Reches and Dewers, 2005), wear and ploughing of the sliding surface (Scholz, 2002), and crushing and thermal expansion of the clasts (Sibson, 1975; Swanson, 1992). Production of small grains during sliding results in an increase of the surface area leading to enhanced grain-to-grain reactivity.

This, coupled with the fact that during seismic slip virtually all the kinetic energy of comminution is converted to heat (Pittarello et al., 2008), facilitates melting. Therefore, bulk melting of ultra-fine-grained granular material can be achieved when it is highly comminuted and strain rate is higher, thus implying that comminution must be a fundamental precursor of melting (Spray, 1995). Field evidence from various tectonic settings of ultracomminuted granular materials associated with earthquakes slip have been recently reported in literature as fluidized gouges (Lin, 1996; Monzawa and Otsuki, 2003, Otsuki et al., 2003; Ujiie et al., 2007; Sagy and Brodsky, 2009) and ultrafine, pulverized rocks (Sagy et al., 2001; Reches and Dewers, 2005; Chester et al., 2005). Fluidization is a deformation mechanism by which granular materials acquire the ability to flow like gas molecules, transmitting stress through intergranular collisions. It is typically described for high shear rates, when granular material lies in the rate-dependent grain-inertia regime (Bagnold, 1954; Campbell, 2006; Lu et al., 2007), and different models have been proposed to account for it (Lachenbruch, 1980; Brune et al., 1993; Melosh, 1996; Brodsky and Kanamori, 2001; Lu et al., 2007).

All these reported fault rocks are ultra-fine-grained and have common microstructures that are also characteristics to BFR granular microlayers (Lin, 1996; Monzawa and Otsuki, 2003, Otsuki et al., 2003; Ujiie et al., 2007; Sagy and Brodsky, 2009). In granular microlayers, grains are extremely small (μm-scale) and exhibit sub-angular to rounded shape. The grain shape suggests preferential abrasion and wearing of the grain corners and that particle rolling dominated over fracturing during faulting. They also show (1) well mixed grains and homogeneous textures, (2) lacking of any indication of slip localization, and, (3) common occurrence of flow structures.

As described in previous sections, BFR layers are extremely hard and cohesive. This observation is also common to other ultra-fine-grained fault rocks (Ujiie et al., 2007; Sagy and Brodsky, 2009), and the cohesiveness is interpreted as due to the increase of the surface area and resulting adhesive forces between grains with ongoing granular deformation (Sagy and Brodsky, 2009).

These similarities suggest mechanisms of ultracomminution, possibly associated with fluidization, to form the granular microtexture of the BFR. An intimate association of fluidized gouges and pseudotachylytes has been reported elsewhere in literature (Otsuki et al., 2003; Monzawa et al., 2003; Kitamura et al., 2005; Ujiie et al., 2007; Sagy and Brodsky, 2009).

6.3 Granular vs. crystalline microlayers: the evolution of seismic slip in the BFR

Granular and crystalline microlayers complexly alternate in each BFR horizon with mutual crosscutting relationships. This intimate association indicates that BFR composite horizons all formed at seismic slip rates. In particular, the analysis of these relationships gives us important constraints on the evolution of these fault rocks during seismic slip.

Microlayers show flow and intrusion structures, and folded or dragged boundaries, comparable to flow banding and folding in volcanic rocks (McPhie et al., 1993). This requires deformation of the whole layer prior to cooling of the pseudotachylyte and solidification of the fluidized ultracomminuted granular material. Moreover, layers are locally truncated and granular microlayers generally cut crystalline microlayers (see truncation of feldspar microlites in Fig. 7C). Frequently, granular microlayers contain many recycled particles of previously formed pseudotachylyte and vice versa. These mutual relationships suggest that each composite BFR horizon records a complex slip history with several slip pulses, each characterized by severe comminution and frictional melting.

Similar millimeter-scale flow structures are reported in a variety of exhumed faults (Otsuki et al, 2003; Monzawa et al., 2003; Kitamura et al., 2005; Ujiie et al., 2007; Sagy and Brodsky, 2009), and complex flow structures have been recently reported in friction experiments performed in non-cohesive materials at seismic slip rates of about 1 m/s (Mizoguchi et al., 2009). Flow structures are interpreted as related to fluidization of granular material or to instabilities between layers with different rheologies, like fluidized gouges and pseudotachylytes (Otsuki et al, 2003; Monzawa et al., 2003, Ujiie et al., 2007). Similarly, flow banding in volcanic rocks is related to laminar flow of lavas with different compositions, viscosities or densities, again implying a difference in mechanical behavior (McPhie et al., 1993). Finally, several examples of volcanic rocks record repeated fracture and healing microstructures, suggesting that magma underwent brittle- and ductile-like deformation during flow and rising in the magmatic conduit (Tuffen et al., 2003 and reference therein).

The presented data, therefore, suggests the occurrence of repeated seismic slip pulses along the BFR. In each single slip event, variably thick layers of ultracomminuted fault rocks formed along the slipping zone (granular microlayers), and some of them were the locus of frictional melt (crystalline or pseudotachylyte-bearing microlayers). The different layers deformed together through flow folding and intrusion structures, yet recording a puzzling and complex deformation history prior to healing of the fault surfaces. The occurrence of fractured microlites even in the crystalline microlayers (pseudotachylytes), in fact, indicates that deformation history ranged in the ductile-brittle transition. The long cooling time (~1000s) suggested by the tabular form of the feldspar microlites would support this long-lived evolution recorded in each BFR composite layer giving the time frame for the variations between solid-like and fluid-like states. Then the presence of reworked clasts in both microlayers, and truncation of pseudotachylyte microlayers by granular ones, suggest that solidification of the BFR microlayers preceded another event of comminution, fluidization and melting.

6.4 BFR vs. cataclasite geochemistry

Textural and petrographic observations clearly indicate that the crystalline microlayers of the BFR are pseudotachylytes (i.e., solidified friction melts). Since the BFR are intimately associated with the cataclasites, with mutual crosscutting relationships (Fig. 3B), we may hypothesize an origin of the pseudotachylytes at the expense of the cataclasite. The BFR have a higher feldspar and Na_2O content compared to the cataclasites, which fits with the occurrence of Na-rich plagioclase microlites in the BFR microcrystalline layers. The presence of albitic microlites in the BFR suggests that friction melting in the cataclasites occurred at the expenses of plagioclase (thus explaining the BFR higher feldspar and Na_2O content compared to the cataclasites). However, the overall mineralogy and geochemistry also show a vastly higher Sr, slightly lower K_2O, Rb and LOI, similar iron oxidation state and MgO, and a non-systematic variation of CaO in the BFR compared to the cataclasites (Figs 10, 11, Tables 1, 2). Therefore, if we take the cataclasite as the source of the BFR, the variations in the geochemistry of the BFR cannot be explained by the selective melting of the phyllosilicates, generally observed in pseudotachylytes (see section 6.1), nor the preferential melting of the plagioclase, nor the bulk melting of the analyzed cataclasite. In the first case, preferential melting of chlorite and illite would result in K_2O, Rb and LOI (probably H_2O) enrichment with respect to the cataclasite. Instead, the strong Sr enrichment of the BFR is at odds with preferential melting of plagioclase, as for plagioclase coexisting with felsic melts, the Sr would remain in the non-melted plagioclase (the partition coefficient between plagioclase and felsic, andesitic/dacitic melts ranges between 2 and 20; http://earthref.org/GERM/), i.e. the BFR should show a lower Sr content than the source rock.

The geochemical relationship between the Pasagshak Point pseudotachylytes and their apparent source rock (i.e., cataclasites) differs greatly from that typically reported in literature. In fact, although total melting of the source rock can be achieved in some pseudotachylytes (e.g., Philpotts, 1964; Obata and Karato, 1995), preferential melting is the most common process, so that the minerals of the host rocks are not proportionately represented among the crystal-fragment population within pseudotachylytes (Shand, 1916; Sibson, 1975; Magloughlin and Spray, 1992; Maddock 1992 see Di Toro et al., 2009 for a recent review). The higher is the degree of host rock melting, the more similar is the composition of the pseudotachylytes to the source rock. The Pasagshak BFR compositions are not well explained by any partial-melting model of the four major minerals in the source rock. Although we cannot fully explain the apparent discrepancies between our observations and previously studied pseudotachylytes, we offer some possible hypotheses that warrant further investigation.

The melting might have been, in this case, non-isochemical, involving loss of material from the slipping zone (i.e., the portion of the fault zone that accommodates the bulk of coseismic shear displacement during an individual rupture event, Sibson, 2003). The occurrence of transient flow of fluids in the cataclasites or along the slipping zone prior to, or right after, pseudotachylyte formation, could represent a means by which removal or addition of cations may occur. It is well established that many accretionary settings at this depth are typically water-saturated, and that fault zones are universally recognized as good pathways for fluids (e.g. Kastner et al., 1991). Moreover, although pseudotachylytes are commonly considered to form under dry conditions (Sibson and Toy, 2006), several examples of fluid circulation, prior (pore fluid) and after (pore fluids and fluids derived from melting of hydrous minerals) pseudotachylyte formation have been described in pseudotachylytes with cataclastic precursors (e.g. Magloughlin, 1989; 1992; 2002 and reference therein; O'Hara and Huggins 2005).

Oscillatory zoning is typically observed in magmatic rocks, where it is classically related to changes in the conditions of crystallization, as abrupt changes in pressure, or to mixing of magmas with different temperature and composition (Shelley, 1992; Hibbard, 1995). Some gradual changes in oscillatory zoning have been related to local effects of disequilibrium crystallization and to the transient variation of water and volatile content in magma (Loomis, 1982; Shelley, 1992). In fact, the *liquidus-solidus* curves for pure anhydrous plagioclase can be depressed by several hundreds of degrees by varying the water content in the system (Shelley, 1992). Therefore, transient fluid flow along the slipping zone and consequent expulsion of material, could explain feldspar crystallization and zoning.

Magloughlin (2002) lists a series of processes possibly influencing the composition of pseudotachylytes, with the alteration of the pseudotachylyte by extensive fluid flow being one of those. Possible evidence of this include the alteration of high-temperature minerals to minerals stable at lower temperature, or growth of new low-temperature minerals in the pseudotachylyte matrix (Magloughlin, 2002, page 28). The occurrence of chlorite and illite in the matrix of crystalline microlayers could suggest alteration of the pseudotachylyte matrix by fluids. Some mobilization of phyllosilicates is necessary also to explain their decrease in the BFR. Therefore, an "open system" during and after pseudotachylyte formation, with the BFR more prone to alteration (possibly fluid-assisted) than the host rock, might be a possible scenario for the formation of the BFR.

Even if we conducted high-resolution microstructural and geochemical (though semi-quantitative as the FE-SEM was equipped with an EDS) analyses, an insight on these issues might come from a detailed geochemical study of the cataclasite and BFR microlayers performed with electron microprobe analysis coupled with FE-SEM. This analytical method would allow, for instance, detailed determination of the composition of the matrix. However, the fine scale layering, that can hamper a selective sampling of granular and crystalline microlayers for analysis, and the fine mixture of microlites and survivor clasts of feldspar in the microlayers, renders this microstructural, mineralogical and chemical investigation extremely challenging.

Lastly, the majority of the pseudotachylytes are hosted in crystalline rocks and produced in other tectonic settings other than the subduction thrust environment observed at Pasagshak Point (Swanson, 1992; Sibson and Toy, 2006 for a review). Therefore, the result of frictional melting in accretionary complexes may not strictly resemble the "typical" pseudotachylyte. The only pseudotachylyte-bearing rocks described in metasediments of equivalent composition and metamorphic grade come from the Shimanto Complex of Japan (Ikesawa et al., 2003; Ujiie et al., 2007), a mélange unit remarkably similar to the Kodiak Island units. Interestingly, Ujiie et al. (2009) performed high velocity rotary friction experiments (seismic slip rates of about 1 m/s) on argillite sampled from the Shimanto belt pseudotachylyte-bearing fault rocks. They produced synthetic pseudotachylytes but, contrary to the typical slip-weakening behavior reported for crystalline host rocks (e.g., Tsutsumi and Shimamoto, 1997; Hirose and Shimamoto, 2005; Di

Toro et al., 2006), in their experiments the slipping zone tend to strengthen with increasing slip. As expecting in slip-strengthening behavior, the slipping zone progressively migrated and the melt layer thickened. This resulted in an anomalously thick slipping zone (up to 0.6 mm), if compared with experiments performed with crystalline rocks (pseudotachylyte thickness < 0.2 mm, e.g., Hirose and Shimamoto, 2005) under similar deformation conditions. Similarly, in nature the BFR average thickness (several cm on fault exposed for hundreds of meters along strike) exceeds the typical mm-scale thickness of pseudotachylytes hosted in crystalline rocks (e.g., Sibson, 1975; 2003; Di Toro et al., 2005). Although Ujiie et al. (2009)'s observations do not solve the problem of the melt source of the BFR, these results emphasize the peculiarity of the pseudotachylytes from exhumed accretionary complexes. Their results suggest that the formation of pseudotachylyte in low-temperature metasediments typical of the seismogenic zone of subduction thrusts may be an essentially different process than the more commonly studied and modeled case of frictional melting along discrete fractures in intact crystalline rocks.

CONCLUSION

The use of high resolution scanning electron microscopy and detailed geochemical characterization established patterns that constrain the origin and possibly the mechanisms of formation of the unusually thick, ultra-fine-grained Pasagshak Point Thrust black fault rocks. We suggest that the BFR are the product of ultracomminution (with possible fluidization) and friction melting of the host cataclasite. The intimate relationship of granular and crystalline (pseudotachylyte-bearing) microlayers indicates that the BFR formed during seismic slip. Therefore, seismic ruptures propagating through and along the cataclasites formed the BFR, which were subsequently altered by interaction with fluids during and after cooling. The BFR horizons, made of multiple composite granular and crystalline microlayers, reach a total thickness of > 30 cm, recording the thickness of the seismic slipping zone during paleoearthquakes on the Pasagshak Point Thrust.

Subduction megathrusts generate the largest earthquakes on Earth. In this contribution, the detailed investigation of the black fault rocks from the fossil subduction thrusts of Pasagshak Point (Alaska) have shed some light on the understanding of how mega thrusts seismic events are recorded and can be recognized in fossil analogues. However, the puzzling geochemical characteristics of BFR when compared to other pseudotachylytes still need to be understood.

Acknowledgements

This work was supported by National Science Foundation Grants OCE-203664 and OCE-0549017 to J. C. Moore. Travel to the U.S. by Francesca Meneghini has been partially supported by Italian MIUR COFIN 2005 Grants to M. Marroni. G. Di Toro was supported by a European Research Council Starting Grant Nr. 205175 (USEMS) and CA.RI.PA.RO. projects. Tim Byrne, Jerry Magloughlin and Associate Editor John Wakabayashi are deeply thanked for their careful revision that improved and strengthen the paper. We particularly thank A. McKiernan and D. Saffer for support during the field campaigns. F. Zorzi and D. Pasqual (University of Padova), provided technical and interpretation support for XRF and XRD data. A. Cavallo is thanked for essential help on FE-SEM analyses at the I.N.G.V. in Rome. L. Pandolfi supported image preparation and quality. Fruitful discussions with E. Brodsky, A. Sagy, T. Byrne, S. Rocchi, S. Agostini and F. Farina greatly improved the quality of this manuscript.

REFERENCES

Allen, A.R., 1979, Mechanism of frictional fusion in fault zones: Journal of Structural Geology, v. 1, p. 231-243.

Bagnold, R.A., 1954, Experiments on a gravity free dispersion of large solid spheres in a Newtonian fluid under shear: Proceedings of the Reological Society of London, v. A225, p. 49–63.

Bilek, S., and Lay, T., 1999, Rigidity variations with depth along interplate megathrust faults in subduction zones: Nature, v. 400, p: 443-446.

Bowden, F.P., and Tabor, D., 1950. The Friction and Lubrication of Solids: Clarendon Press, Oxford, United Kingdom, 337 p.

Brodsky, E. E., and Kanamori, H., 2001, Elastohydrodynamic lubrication of faults: Journal of Geophysical Research, v. 106, 16357–16374.

Brodsky, E.E., Rowe, C.D., Meneghini, F., and Moore, J.C., 2009, A geological fingerprint of low-viscosity fault fluids mobilized during an earthquake: Journal of Geophysical Research, v. 114, p. B01303, doi: 10.1029/2008JB005633.

Brune, J.N., Brown, S., and Johnson, P.A., 1993, Rupture mechanism and interface separation in foam rubber models of earthquakes: a possible solution to heat flow paradox and the paradox of large overthrusts: Tectonophysics, v. 218, p. 59– 67.

Byrne, T., 1982, Structural evolution of coherent terranes in the Ghost Rocks Formation, Kodiak Island, Alaska: Geological Society of London Special Publication 10, p. 229-242.

Byrne, T., 1984, Early deformation in mélange terranes of the Ghost Rocks Formation, Kodiak Islands, Alaska, *in* Raymond, L.A., ed., Mélanges: their nature, origin and significance: Geological Society of America Special Paper 198, p. 21-52.

Campbell, C.S., 1993, Boundary interactions for two-dimensional granular flows: Part I. Flat boundaries, asymmetric stresses and couple stresses: Journal of Fluid Mechanics, v. 247, p. 111-136.

Campbell, C.S., 2006, Granular material flows - an overview: Powder Technology, v. 162, p. 208–229.

Carslaw, H.S., and Jaeger, J.C., 1959, Conduction of Heat in Solids, 2nd edition, Oxford at the Clarendon Press, Oxford.

Chester, J.S., Chester, F.M., and Kronenberg, A.K., 2005, Fracture surface energy of the Punchbowl fault, San Andreas system: Nature, v. 437, doi:10.1038/nature03942.

Corrigan, G.M., 1982, The crystal morphology of plagioclase feldspar produced during isothermal supercooling and constant rate experiments: Mineralogical Magazine, v. 46, p. 433-439.

Cowan, D. S., 1999, Do faults preserve a record of seismic slip? A field geologist's opinion: Journal of Structural Geology, v. 21, p. 995-1001.

Craddock, J. P., and Magloughlin, J. F., 2005, Calcite strains, kinematic indicators, and magnetic flow fabric of a Proterozoic pseudotachylyte swarm, Minnesota River valley, USA: Tectonophysics, 402, p. 153– 168.

Di Toro, G., and Pennacchioni, G., 2004, Superheated friction-induced melts in zoned pseudotachylytes within the Adamello tonalites (Italian Southern Alps): Journal of Structural Geology, v.26, p. 1783–1801.

Di Toro, G., Nielsen, S., and Pennacchioni, G., 2005, Earthquake rupture dynamics frozen in exhumed ancient faults: Nature, v. 446, p. 1009-1012, doi: 10.1038/nature03910.

Di Toro, G., Hirose, T., Nielsen, S., Pennacchioni, G., and Shimamoto, T., 2006. Natural and experimental evidence of melt lubrication of faults during earthquakes: Science, v. 311, p. 647-649.

Di Toro, G., Pennacchioni G., and Nielsen, S., 2009. Pseudotachylytes and Earthquake Source Mechanics, *in* Fukuyama, E., ed., Fault-zone Properties and Earthquake Rupture Dynamics, International Geophysics Series, Elsevier, Amsterdam, The Netherlands, in press.

Fialko, Y., and Khazan, Y., 2005, Fusion by earthquake fault friction: Stick or slip?: Journal of Geophysical Research, v. 110, p. B12407, doi: 939 10.1029/2005JB003869.

Fisher, D., and Byrne, T., 1987, Structural evolution of underthrusted sediments, Kodiak Islands, Alaska: Tectonics, v. 6, no. 6, p. 775-793.

Haeussler, P. J., Bradley, D. C., Wells, R., and Miller, M. L., 2003, Life and death of the Resurrection plate: Evidence for its existence and subduction in the northeastern Pacific in Paleocene-Eocene time: Geological Society of America Bulletin, v. 115, no. 7, p. 867-880.

Hibbard, M.J., 1995, Petrography to Petrogenesis: Prentice Hall, Englewood Cliffs, New Jersey, pp 587.

Hirose, T., and Shimamoto, T., 2005, Growth of molten zone as a mechanism of slip weakening of simulated faults in gabbro during frictional melting: Journal of Geophysical Research, v. 110, B05202, doi:10.1029/2004JB003207.

Ide, S., and Takeo, M., 1997, Determination of constitutive relations of fault slip based on seismic wave analysis: Journal of Geophysical Research, v. 102, no. B12, p. 27,379–27,391.

Ikesawa, E., Sagaguchi, A. and Kimura, G., 2003, Pseudotachylyte from an ancient accretionary complex: Evidence for melt generation during seismic slip along a master décollement?: Geology, v. 31, no. 7, p. 637–640.

Jaeger, J.C., 1968. Cooling and solidification of igneous rocks, *in*: Hess, H.H., Poldevaart, A., eds., Basalts, Vol. 2.: Interscience Publishers, New York, pp. 503 – 536.

Kastner, M., Elderfield, H., and Martin, J.B., 1991, Fluids in convergent margins: what do we know about their composition, origin, role in diagenesis and importance for oceanic chemical fluxes?, *in*: Tarney J., Pickering K.T., Knipe J. and Dewey J.F., eds., Fluids in subduction zones. Philosophical Transactions of the Royal Society, London, v. A335, 17-34.

Kitamura, Y., Sato, K., Ikesawa, E., Ikehara-Ohmori, K., Kimura, G., Kondo, H., Ujiie, K., Onishi, C. T., Kawabata, K., Hashimoto, Y., Mukoyoshi, H., and Masago, H., 2005, Melange and its seismogenic roof decollement: A plate boundary fault rock in the subduction zone - An example from the Shimanto Belt, Japan: Tectonics, v. 24, TC5012, doi: 10.1029/2004TC001635, p. 15.

Lachenbruch, A.H., 1980, Frictional heating, fluid pressure, and the resistance to fault motion: Journal of Geophysical Research, v. 85, p. 6249–6272.

Lin, A., 1996, Injection veins of crushing-originated pseudotachylyte and fault gouge formed during seismic faulting: Engineering Geology, v. 43, p. 213-224.

Lin, A., 2008 Fossil earthquakes: the formation and preservation of pseudotachylytes, Springer, Berlin, 348 pp.

Lesher, C.E., Cashman, K.V., and Mayfield, J.D., 1999, Kinetic controls on crystallization of Tertiary North Atlantic basalt and implications for the emplacement and cooling history of lava at Site 989, Southeast Greenland rifted margin, *in* Larsen H.C., Duncan R.A., Allan J.F., and Brooks, K., eds., Proceeding of the ODP, Scientific Results, 163, College Station, Texas (Ocean Drilling Program), p. 3-16.

Lofgren, G., 1974, An experimental study of plagioclase crystal morphology: isothermal crystallization: American Journal of Science, v. 274, p. 243-273.

Lofgren, G., 1980, Experimental studies on the dynamic crystallization of silicate melts, *in* Hargraves R.B., ed., Physics of Magmatic processes: Princeton University Press, Princeton, p. 487-551.

Loomis, T.P., 1982, Numerical simulations of crystallization processes of plagioclase in complex melts; the origin of major and oscillatory zoning in plagioclase: Contributions to Mineralogy and Petrology, v. 81, no. 3, p. 219-229.

Lu, K., Brodsky, E., and Kavehpour, H.P., 2007, Shear-weakening of the transitional regime for granular flow: Journal of Fluid Mechanics, v. 587, p. 347-372, doi: 10.1017/S0022112007007331 347.

McPhie, J., Doyle, M., and Allen, R., 1993, Volcanic textures. A guide to the interpretation of textures in volcanic rocks: Centre for Ore Deposit and Exploration Studies, University of Tasmania, Hobart, Tasmania, pp 967.

Maddock, R. H., 1983, Melt origin of fault-generated pseudotachylytes demonstrated by textures: Geology, v. 11, p. 105-108.

Maddock, R.H., 1986, The petrology and geological significance of some fault-generated pseudotachylytes. Unpublished Ph.D. thesis, University of London, London, 423 pp.

Maddock, R.H., 1992, Effects of lighology, cataclasis and melting on the composition of fault-generated pseudotachylytes in Lewisian gneiss, Scotland: Tectonophysics, v. 204, p. 261-270.

Magloughlin, J. F., 1992, Microstructural and chemical changes associated with cataclasis and frictional melting at shallow crustal levels: the cataclasite-pseudotachylyte connection: Tectonophysics, v. 204, p. 243-260.

Magloughlin, J. F., 2002, An evaluation of Rb-Sr dating of pseudotachylyte: Structural-chemical models and the role of fluids. Geochemical Journal, v. 37, p. 21-33.

Magloughlin, J. F., and Spray, J. G., 1992, Frictional melting processes and products in geologic materials: introduction and discussion: Tectonophysics, v. 204, p. 197-206.

Melosh, H.J., 1996, Dynamic weakening of faults by acoustic fluidization: Nature, v. 397, p. 601–606.

Mizoguchi, K., Hirose, T., Shimamoto, T. and Fukuyama, E., 2009, High-velocity frictional behavior and microstructure evolution of fault gouge obtained from Nojima fault, southwest Japan: Tectonophysics**,** v. 471, p. 285-296.

Monzawa, N., and Otsuki, K., 2003, Comminution and fluidization of granular fault materials: implications for fault slip behavior: Tectonophysics, v. 367, p. 127-143.

Moore, G. W., 1969, New formations on Kodiak and adjacent islands, Alaska: USGS Bulletin, v. 1274-A, p. A27-A35.

Moore, J.C. and Allwardt, A., 1980, Progressive deformation of a Tertiary trench slope, Kodiak Islands, Alaska: Journal of Geophysical Research, v. 85, p. 4741-4756.

Nielsen, S., Di Toro, G., Hirose, T., and Shimamoto, T., 2008, Frictional melt and seismic slip: Journal of Geophysical Research, v. 113, p. B01308, doi: 10.1029/2007JB0051222008.

Obata, M. and Karato, S., 1995, Ultramafic pseudotachylite from the Balmuccia peridotite, Ivrea-Verbano zone, northern Italy: Tectonophysics, v. 242, p. 313-328.

O'Hara, K. D., and Huggins, F. E., 2005, A Mossbauer study of pseudotachylytes: redox conditions during seismic faulting: Contributions to Mineralogy and Petrology, v. 148, p. 602-614.

Otsuki, K., Monzawa, N., and Nagase, T., 2003, Fluidization and melting of fault gouge during seismic slip: Identification in the Nojima fault zone and implications for focal earthquake mechanisms: Journal of Geophysical Research, v. 108, p. B42192, doi: 10/1029/2001JB001711.

Philpotts, A. R., 1964, Origin of Pseudotachylites: American Journal of Science, v. 262, p. 1008-1035.

Philpotts, A. R., 1982, Compositions of immiscible liquids in volcanic rocks: Contributions to Mineralogy and Petrology, v. 80, p. 201– 218.

Philpotts, A.R. and Miller, J.A., 1963, A Pre-Cambrian glass from St. Alexis-des-Monts, Quebec: Geological Magazine, v. 100, p. 337-344.

Pittarello, L., Di Toro, G., Bizzarri, A., Pennacchioni, G., Hadizadeh, J., and Cocco, M., 2008, Energy partitioning during seismic slip in pseudotachylyte-bearing faults (Gole Larghe Fault, Adamello, Italy): Earth and Planetary Science Letters, v. 269, no. 1-2, p. 131-139.

Plafker, G., Moore, J. C., and Winkler, G. R., 1994, Chapter 12: Geology of the southern Alaska margin, *in* Plafker, G., and C., B. H., eds., The Geology of Alaska: The Geology of North America, p. 389-449. Geological Society of America, Boulder, CO, U.S.A.

Reches, Z.E., and Dewers, T.A., 2005, Gouge formation by dynamic pulverization during earthquake rupture: Earth and Planetary Science Letters, v. 235, p. 361-374.

Rice J.R., 2006, Heating and weakening of fault during earthquake slip: Journal of Geophysical Research 111, p. B05311, doi:10.1029/2005JB004006.

Roeske, S.M., Mattinson, J.M., and Armstrong, R.L., 1989, Isotopic ages of glaucophane schists on the Kodiak Islands, southern Alaska, and their implications for the Mesozoic tectonic history of the Border Ranges Fault system: Geological Society of America Bulletin, v. 101, p. 1021-1037.

Rowe, C. D., Moore, J. C., Meneghini, F., and McKiernan, A. W., 2005, Large-scale pseudotachylytes and fluidized cataclasites from an ancient subduction thrust fault: Geology, v. 33, p. 937–940, doi: 10.1130/G21856.1.

Rowe, C. D., 2007, Snapshots of the Earthquake Cycle: An Approach to Subduction Zone Paleoseismicity. Unpublished Ph.D., University of California, Santa Cruz, 185 pp.

Sagy, A., Reches, Z.E., and Roman, I., 2001, Dynamic fracturing: field and experimental observations: Journal of Structural Geology, v. 23, p. 1223-1239.

Sagy, A., and Brodsky, E.E., 2009, Geometric and rheological asperities in an exposed fault zone: Journal of Geophysical Research, v.114, p. B02301, doi: 10.1029/2008JB005701.

Sample, J.C., and Moore, J.C., 1987, Structural style and kinematics of an underplated slate belt, Kodiak and adjacent islands, Alaska: Geological Society of America Bulletin, v. 99, p. 7-20.

Sample, J.C., and Reid, M., 2003, Large-scale, latest Cretaceous uplift along the northeast Pacific Rim: evidence from sediment volume, sandstone petrography and Nd isotope signatures of the Kodiak Formation, Kodiak Islands, Alaska, *in* Sisson, V.B., Roeske, S.M., and Pavlis, T.L., eds, Geology of a transpressional orogen developed during ridge-trench interaction along the North Pacific margin: Geological Society of America Special Paper 371, p. 51-70.

Scholz, C.H., 2002, The mechanics of earthquakes and faulting – 2nd edition: Cambridge Press, New York, 496 pp.

Shand, S.J., 1916, The pseudotachylyte of Parijs (Orange Free State) and its relation to “trap-shotten gneiss” and “flinty crush rock”: Quarterly Journal of the Geological Society of London, v. 72, p. 198-221.

Shelley, D., 1992, Igneous and metamorphic rocks under the microscope; classification, textures, microstructures and mineral preferred-orientations. Part two: Textures and Microstructures: Chapman and Hall, London, UK, 445 pp.

Sibson, R.H., 1975, Generation of pseudotachylyte by ancient seismic faulting: Geophysical Journal of the Royal Astronomical Society, v. 43, p. 775-794.

Sibson, R.H., 2003, Thickness of the Seismic Slip Zone: Bulletin of the Seismological Society of America, v. 93, p. 1169-1178.

Sibson, R.H. and Toy, V., 2006, The habitat of fault-generated pseudotachylyte: presence vs. absence of friction-melt, *in* Abercrombie, R., McGarr, A., Di Toro, G., and Kanamori, H., eds., Radiated Energy and the Physics of Faulting: Geophysical Monograph Series 170, p. 153-166, American Geophysical Union, Washington, D.C.

Smith J.V. and Brown, W.L., 1988, Feldspar Minerals: Crystal Structures, Physical, Chemical, and Microtextural Properties: Springer Verlag, Berlin, 852 pp.

Snoke A.W., Tullis J., Todd V.R. (Eds.), Fault Related Rocks. A photographic Atlas: Princeton University Press, New Jersey, 629 pp.

Spray, J.G., 1987, Artificial generation of pseudotachylyte using friction welding apparatus: simulation of melting on a fault plane: Journal of Structural Geology, v. 9, p. 49-60.

Spray, J.G., 1992, A physical basis for the frictional melting of some rock-forming minerals: Tectonophysics, v. 204, p. 205-221.

Spray, J.G., 1995, Pseudotachylyte controversy: fact or friction?: Geology v. 23, p. 1119-1122.

Swanson, M.T., 1992, Fault structure, wear mechanisms and rupture processes in pseudotachylyte generation: Tectonophysics, v. 204, p. 223-242.

Tsutsumi, A., and Shimamoto, T., 1997, High-velocity frictional properties of gabbro: Geophysical Research Letters, v. 24, p. 699-702.

Tsutsumi, A., Rowe, C.D., Moore, J.C., Meneghini, F., and Yamaguchi, A., 2008, High velocity frictional properties of subducting materials: An example study for argillaceous mélange rock: Abstract volume of the Japan Geoscience Union Meeting, J163-002.

Tuffen, H., Dingwell, D.B., and Pinkerton, H., 2003, Repeated fracture and healing of silicic magma generate flow banding and earthquakes?: Geology, v. 31, v. 1089-1092.

Ujiie, K., Yamaguchi, A., Kimura G., and Toh, S., 2007, Fluidization of granular material in a subduction thrust at seismogenic depths: Earth and Planetary Science Letters, v. 259, p. 307–318.

Ujiie, K., Tsutsumi, A., Fialko, Y., and Yamaguchi, H., 2009, Experimental investigation of frictional melting of argillite at high slip rates: implications for seismic slip in subduction-accretion complexes: Journal of Geophysical Research, v.114, no. B04308, doi:10.1029/2008JB006165.

Vrolijk, P., Myers, G., and Moore, J. C., 1988, Warm fluid migration along tectonic melanges in the Kodiak Accretionary Complex, Alaska: Journal of Geophysical Research, v. 93, no. B9, p. 10,313-10,324.

Wibberley , C.A.J, Graham, Y., and Di Toro, G., 2008, Recent advances in the understanding of fault zone internal structure: a review, *in* Wibberley, C.A.J., Kurz, W., Imber, J., Holdsworth, R.E., and Collettini, C., eds., The Internal Structure of Fault Zones – implications for mechanical and fluid flow properties: Geological Society of London Special Volume 299, p. 5-33.

FIGURES

Figure 1. Simplified geologic maps of (A) Kodiak Island and (B) Pasagshak Point. Inset in B shows location of Kodiak Island with respect to the State of Alaska. Line segments a-d refer to location of cross section of Figure 2. The names of the selected outcrops where detailed structural analyses and sampling were conducted are noted in italics. Kodiak map after Fisher and Byrne (1987).

Figure 2. Schematic structural section across Pasagshak Point peninsula (see trace of cross section in Figure 1). The three BFR-bearing cataclastic shear zones are shown.

Figure 3. End-member meso-scale features in cataclasite. (A) Clast-rich foliated and (B) non-foliated cataclasites. Foliated cataclasites also show complex folding, with asymmetric thrust-related folds. Non-foliated cataclasites contains frequently reworked rounded fragment or ribbons of fine-grained black fault rocks (BFR). Lens cape diameter in (B) is 4.5 cm.

Figure 4. Field classification of BFR. Since most of the best-exposed BFR's occur in foliated cataclasites, we generally refer to this group of textures when using the term cataclasites (CC) in pictures. (A) and (B) Typical BFR field occurrences with BFR cutting at a low angle through the cataclasites. (A) BFR at outcrop WPT015 (see location in Figure 1). Footwall is fine-grained foliated cataclasite (CC), while the hangingwall is represented by a sandstone-rich section of the mélange (SST). The two end member field classes of BFR textures are also shown: BFR-aph are aphanitic layers and BFR-grs are grain-supported layers. White dashed lines mark BFR boundaries. Photo is oblique section looking toward the NW. (B) BFR at outcrop WPTBLKSTF (see location in Figure 1). Footwall is foliated cataclasite, while coarse-grained cataclasite rich in greenstone and sandstone boudins (gs) characterizes the hangingwall. Hangingwall cataclasites also show asymmetric thrust-related folding (solid white line) with transport to the southeast. Dashed white lines mark BFR boundaries. Photo is taken looking toward the NW. (C) Close up view of aphanitic layer from the BFR horizon shown in (B), with the characteristic satin luster. Dashed white line mark BFR lower boundary. Lens cape diameter is 4.5 cm. Photo is taken looking toward the W. (D) Close up view of grain-supported layer (BFR-grs), alternating with aphanitic layers (BFR-aph), from BFR layer of (A). Thick solid white line mark BFR lower boundary; thin dashed line runs through aphanitic and grain-supported layers boundary. Lens cape diameter is 5 cm. Photo is oblique section and faces the W.

Figure 5. BFR/host rock relationships. (A) BFR lower boundary (lower white dashed line) is always sharp and subplanar, cutting the cataclasite (CC) fabric at a low angle; outcrop WPT015 (see location in Figure 1). At the centimeter-scale both grain-supported (BFR-grs) and aphanitic (BFR-aph, boundaries with solid white lines) layers are recognized; aphanitic layers are more resistant to weathering. SST in figure refers to sandstone blocks in cataclasite mappable at outcrop scale (B) Injection vein (inj) with sharp walls into overlying sandstone (SST). (C) Decimeter-scale intrusions of black layer into cataclasite (sketch of photo in the inset). Mixing with overlying cataclasite also occurs and cataclasite deforms ductile in close proximity of intrusions. Lens cape diameter is 4.5 cm.

Figure 6. BFR microstructure. Although microscale observation confirm similarly to what observed in the field, an internal layering of BFR, alternation of two different microtextures only occur in the aphanitic layers. Therefore, while grain-supported layers only show one type of microtexture, the aphanitic layers show the microlayering shown here and described in main text. (A) Optical plane light image (PPL) of BFR internal layering in a BFR sample characterized at field scale by aphanitic tecture. BFR-cx crystalline microlayers, include few large quartz grains (bright subrounded grains in figure), and are enriched in chlorite and clay minerals with respect to BFR-gr granular microlayers. Granular microlayers have a granular aspect due to a concentration of quartz grains in an irresolvable matrix. In granular microlayers, reworked clasts BFR-cx material are also visible (darker spots pointed by white arrows). Later pressure solution seams are ubiquitous (ps with white arrows), similarly to what observed by Magloughlin (1989, fig.5c), though they seem to concentrate in the BFR-gr microlayers. Boundary between layers can be sharp and marked by pressure solution, as the lower left boundary of BFR-gr microlayer, or gradational as the BFR-gr microlayer upper right boundary in picture. (B) Same layering as in (A) in SEM-BSE imagery: BFR-cx crystalline microlayer to the right shows a higher chlorite (medium gray colors in picture) content with respect to the gray BFR-gr microlayer to the left. BFR-gr microlayers matrix show higher variability in grain size than BFR-cx crystalline microlayers. In the crystalline microlayers the matrix is defined essentially by chlorite wrapped around a framework of almost equidimensional sub-rounded quartz and plagioclase grains. The contact between granular and crystalline microlayers in this image is planar and very sharp, except for the quartz (qtz) grain from crystalline microlayer on the right that is indenting into the granular microlayer. (C) High resolution FE-SEM image of layering in BFR (BSE): BFR-cx

bright microlayer is crystalline and characterized by a matrix of quartz (qtz) and complexly zoned euhedral albitic plagioclase (pl), up to a few μm long, coated by sub-μm grains of chlorite and illite (white minerals). Phyllosilicates makes up to the 20% of this layer. Granular BFR-gr microlayers are made by an arrangement of quartz and feldspars clasts showing higher grain size variability than BFR-cx microlayers. Matrix phyllosilicates here represent up to the 10% of the investigated area (see also Fig. 6F). Note also the spectacular higher resolution of FE-SEM image compared to the SEM image in (B). (D) Close up view of the BFR-cx crystalline microlayer. High-resolution enables imaging of μm –scale tabular plagioclases with normal (nzp), reverse (rzp) and oscillatory (ozp) zoning, as well as chlorite and minor illite (white platy minerals in figure) arranged in the matrix between the plagioclase and quartz (qtz). White arrow indicates crushed feldspar, locally observed in the crystalline microlayers. (E) Embayment on quartz grains in crystalline microlayer, with chlorite wrapped around clast. Note the presence of several crushed zoned microlites of plagioclase. (F) Close-up view of BFR-gr granular microlayer of picture (A). Microgranular layers are poorly sorted, with quartz (qtz) and plagioclase (pl), often in fragments, producing a matrix covering all ranges of grain size from 2 μm to sub-μm. The content of chlorite and illite (< 10% of the total area) dramatically decreases with respect to the microcrystalline layer. Scattered bright Ti-oxides and Fe-sulfides are common in the two layer types, with also comparable abundance (sub-rounded bright, shining white grains in Figure D and F).

Figure 7. Grain contouring of (A) BFR-crystalline and (B) BFR-granular microlayers. Images used are those of Figs. 6D and 6F, respectively. Big, clearly zoned plagioclases are distinguished with a medium gray color. Quartz, and plagioclase grains smaller than 1 μm or those that cannot be identified easilyas zoned, are not distinguished in the contour and are all indicated with the dark gray color. White grains are undifferentiated oxides and sulfides, while light gray spots are undifferentiated phyllosilicates. The black patches are holes: though most of them look like primary porosity, some might also be the result of sample preparation. As described in the text, BFR granular microlayers show a higher packed texture with quartz and plagioclase grains frequently in contact. Grain size variability is higher in the granular microlayers than the crystalline microlayers, while the phyllosilicate content decrease from 10-20% in the crystalline microlayers to below the 10% in the granular layers. Zoned plagioclase concentrate in crystalline microlayers.

Figure 8. Crosscutting relationships between different BFR layers. (A) Clasts of the crystalline microlayers (BFR-cx) are frequently found in granular microlayers (BFR-gr). (B) Clasts of the granular microlayers (BFR-gr) are found in crystalline microlayers (BFR-cx). (C) Close up view of a granular microlayer (BFR-gr) cutting sharply a crystalline microlayer (BFR-cx). Broken plagioclases are found along the contact between the two layers (white arrow). This observation implies that plagioclase in the crystalline microlayer was already crystallized when granular microlayer formed, providing a local relative chronology of events. (D) Optical microscope plane light image of flow structures between crystalline and granular microlayers, resembling those described in volcanic rocks (McPhie et al., 1993) and in pseudotachylytes (Magloughlin 1989; 1992; 2005; Craddock and Magloughlin, 2005). The granular microlayer to the bottom hosts several anastamosing, black in color, pressure solution seams. (E) Injection veins are locally found, usually when the hanging wall of BFR is made of sandstone-rich sections of the mélange. Sketch of photo in the inset.

Figure 9. Microstructures in cataclasites. (A) Optical microscope plane light image of a foliated cataclasite. Quartz and sandstone (sst) clasts are wrapped by a penetrative foliation (S) defined by the preferred orientation of phyllosilicate grains and by pressure solution seams (ps). (B) Foliated cataclasites under the high resolution FE-SEM (BSE). Note the presence of angular to sub-rounded shaped quartz (qz) and plagioclase (pl) clasts, and the absence of tabular or zoned feldspars. The shaped preferred orientation of phyllosilicates (chlorite and illite) along the NE-SW diagonal of image, define a penetrative scaly foliation (S).

Figure 10. Composition (X-Ray Fluorescence analyses) of the Pasagshak Point fault rocks. (A) At each selected outcrop, we made transects across the BFR and collected samples with a rock drill from the footwall, the BFR, and the hanging wall (white open circles). Depending on the BFR thickness, we collected one or more samples, at the BFR layer center and at 3, 10 and 30 cm down-section and up-section from the BFR cataclasite-boundary. Lens cape diameter is 5 cm. (B) X-Ray Fluorescence analytical data: BFR bulk composition normalized to that of cataclasite for major oxides (in %, right image) and minor elements (in ppm, left image) (see Table 1 and main text for description).

Figure 11. Mineralogy of the cataclasites and BFR from Pasagshak Point. (A) Powder X-ray diffraction spectra of bulk BFR compared with bulk cataclasites from both hanging wall and footwall for transect at outcrop WPT014. Sample names are reported on the upper left spectra:

PP80-cataclasite from footwall of BFR; PP77–BFR; PP83–cataclasite from hanging wall of BFR. Though the mineral assemblage is similar, the qualitative comparison of peak intensities indicate that BFRs are clearly enriched in plagioclase and slighly depleted in phyllosilicates (illite) with respect to the cataclasite. (B) Where possible, crystalline and granular microlayers were separated and analyzed. As shown in the reported powder X-ray diffraction spectra, by comparing the microlayers spectra with those of Figure 11A, the crystalline microlayers (PP113gl, cx BFR) have a modal composition similar to that of the bulk BFR (higher feldspar and lower phyllosilicate/chlorite content with respect to cataclasisites), whereas the granular microlayers (PP113gr, gr BFR) have a modal composition more similar to that of the cataclasites. Minerals abbreviations: pl – feldspars; qtz – quartz; chl – chlorite; phyl – phyllosilicate peak (illite group). While the peaks for phyllosilicate include the whole mica group, previous detailed XRPD analyses have shown that only illite is present in these samples (Rowe, 2007).

Figure 12. Cooling history (see Eq. 1) at the centre of a melt layer, with an initial temperature of 1100^{o}C, hosted in a host rock at 250^{o}C, according to Eq. 1. The three curves represent melt layers of 1, 6 and 8 cm of thickness, respectively. Note the abrupt cooling of a 1-cm thick melt layer (typical thickness of pseudotachylytes fault veins from intra-continental setting, e.g., Di Toro et al., 2005), compared to a 6 to 8 cm thick vein (typical thickness of pseudotachylytes from the subduction setting of the Pasagshak point). Feldspar microlites in cm-thick pseudotachylytes are usually acicular and bow tie (e.g., Lin, 1994; Fabbri et al., 2000; Di Toro and Pennacchioni, 2004). The slower cooling rate of the exceptionally thick pseudotachylytes from Pasagshak Point may explain the tabular shape of the feldspar microlites.

Table 1 – (Bulk) chemical composition of BFR and associated cataclasites (CC) analyzed by X-ray fluorescence are reported here for two selected outcrops, wpt014 and wpt015. See map in Figure 1 for outcrops location.

Table 2 – Average chemical compositions and standard deviations, along the studied fault zone exposure, of cataclasite and BFR. Since the BFR sample of WPT009 shows an anomalously higher increase in Sr than the cataclasites compared to other outcrops, the average and standard deviation values without this sample have been recalculated and are shown in brackets.

Figure 1
Click here to download high resolution image

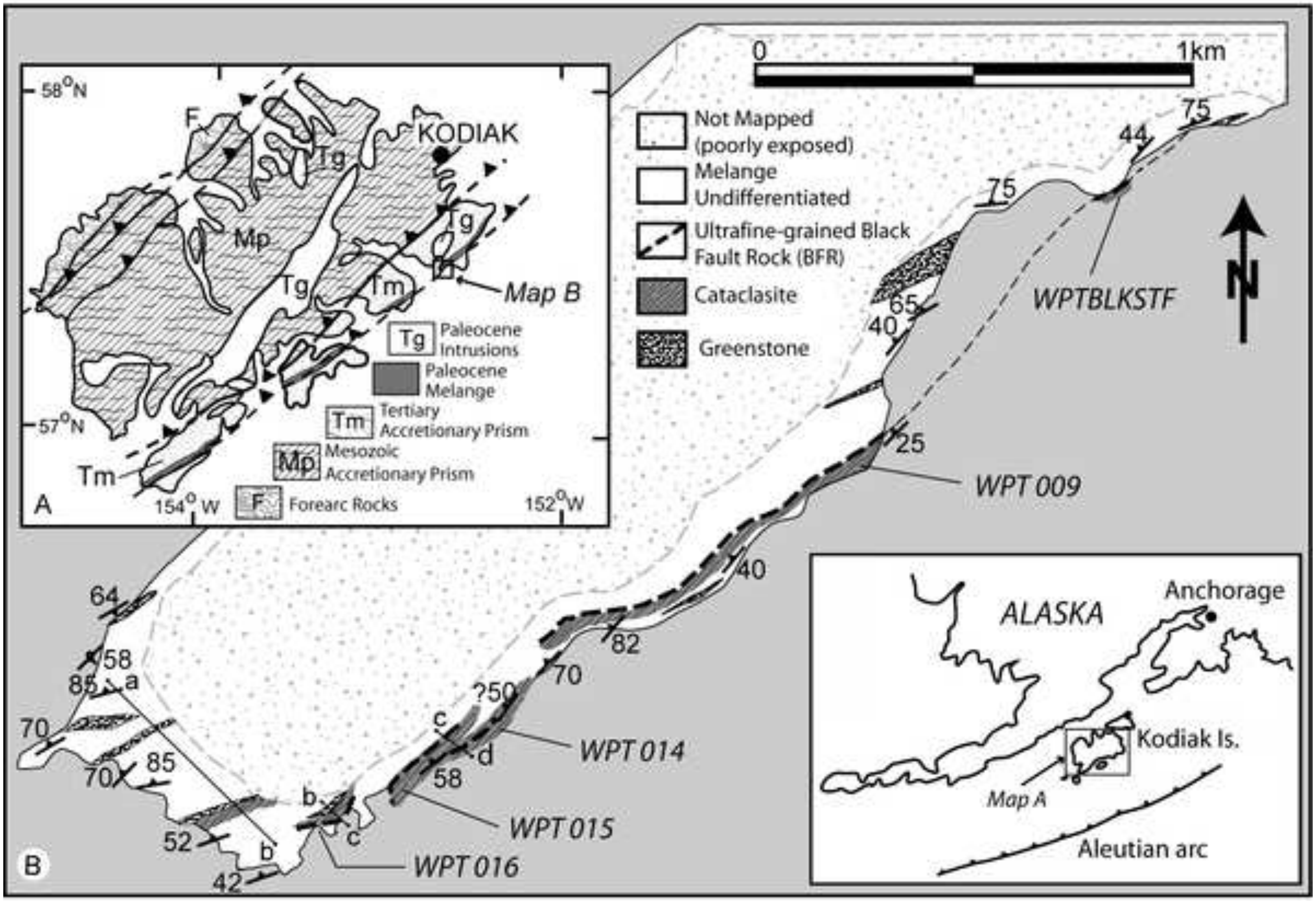

MENEGHINI ET AL. - FIGURE 1

Figure 2
Click here to download high resolution image

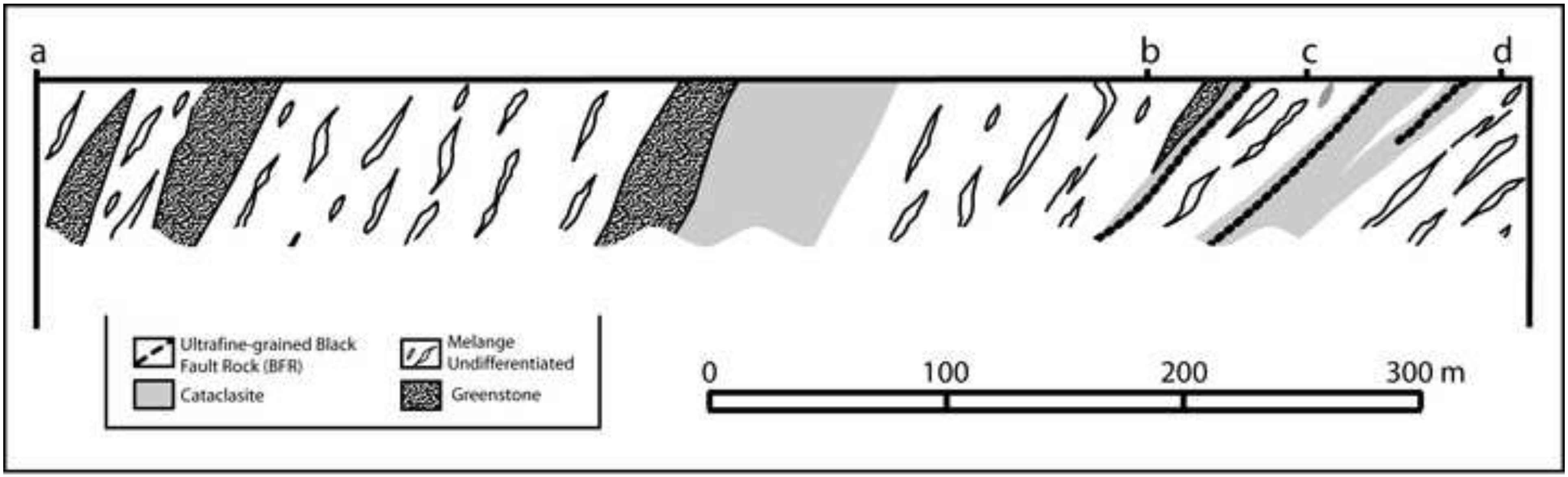

MENEGHINI ET AL. - FIGURE 2

Figure 3
Click here to download high resolution image

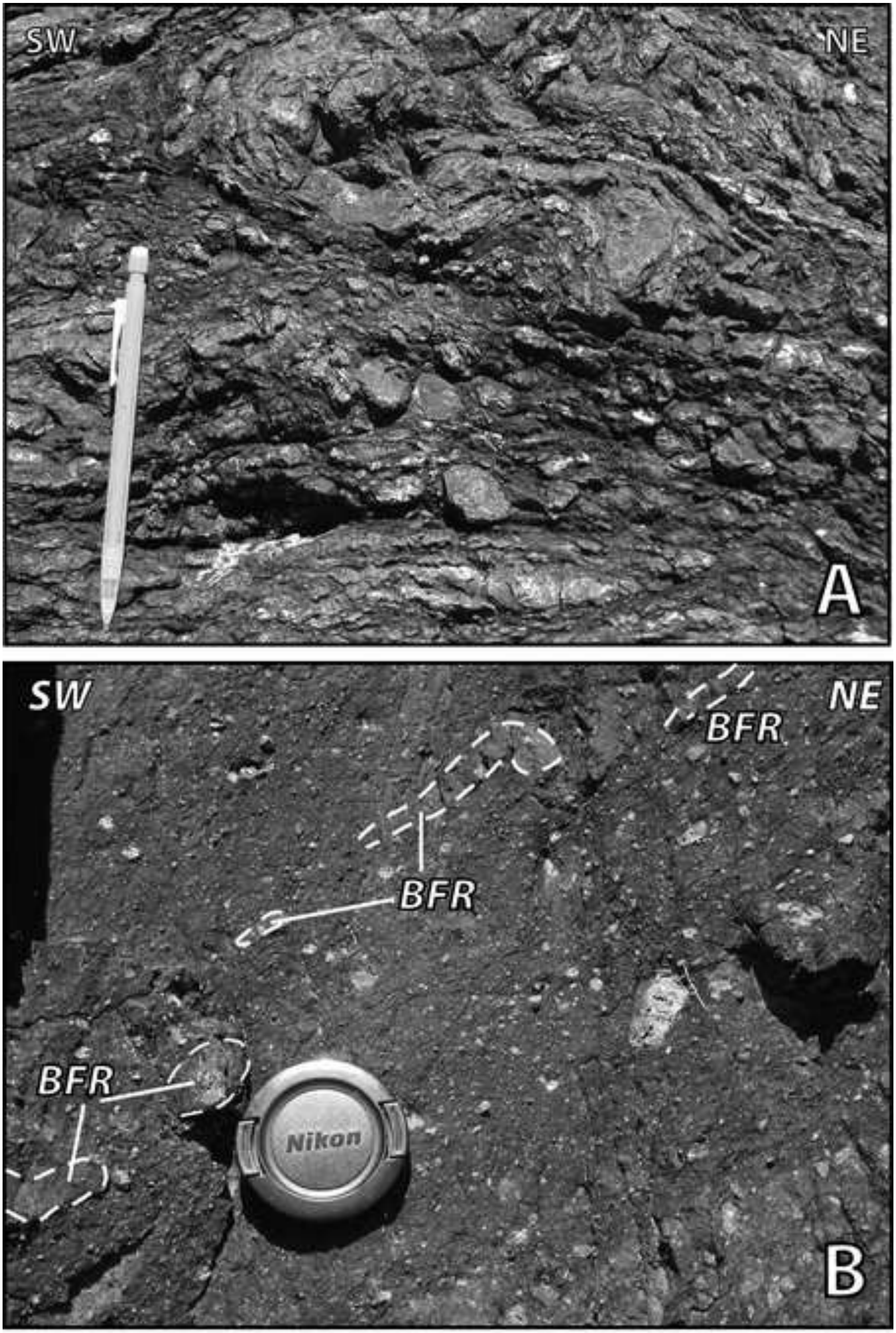

MENEGHINI ET AL. - FIGURE 3

Figure 4
Click here to download high resolution image

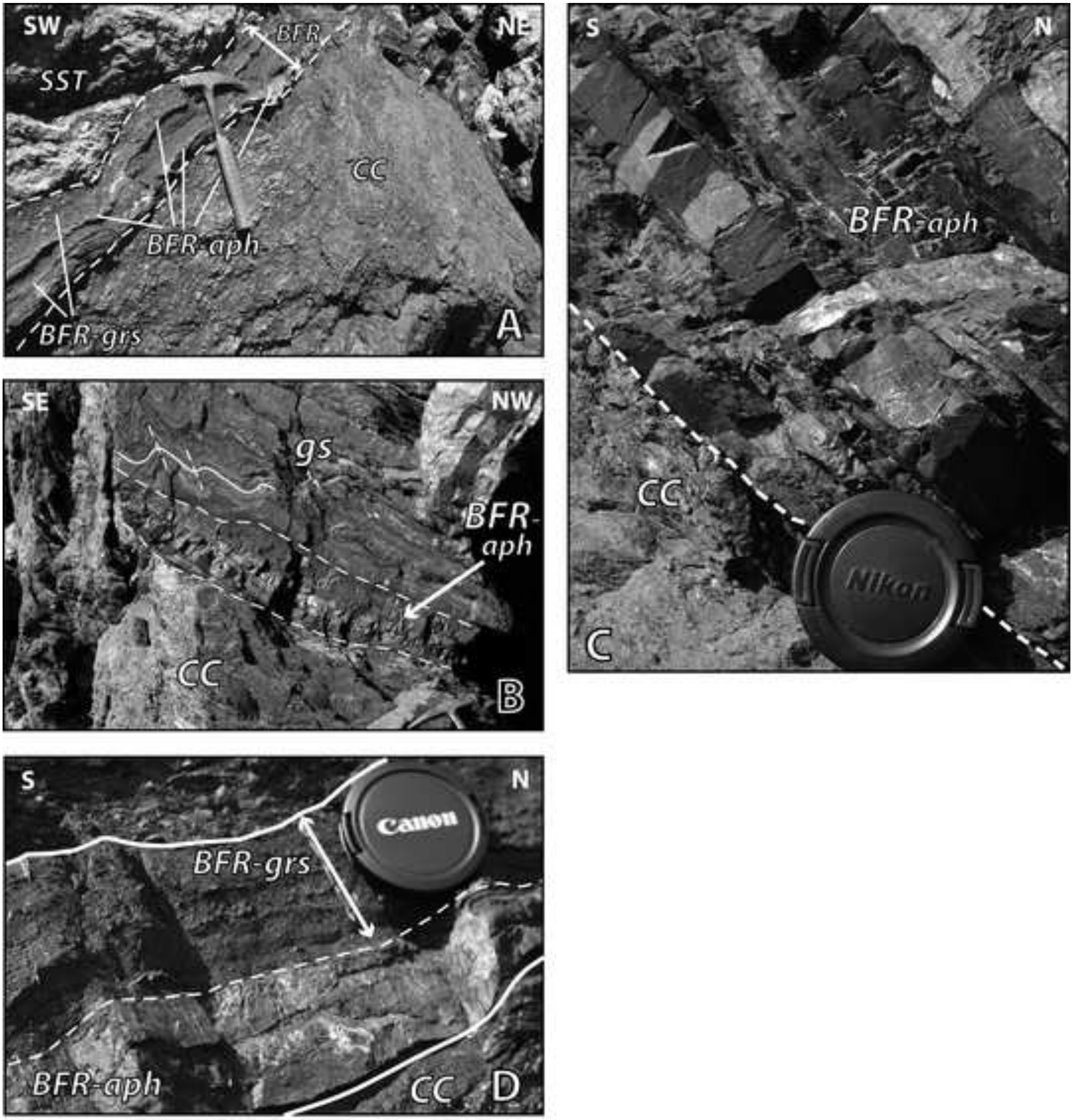

MENEGHINI ET AL. - FIGURE 4

Figure 5
Click here to download high resolution image

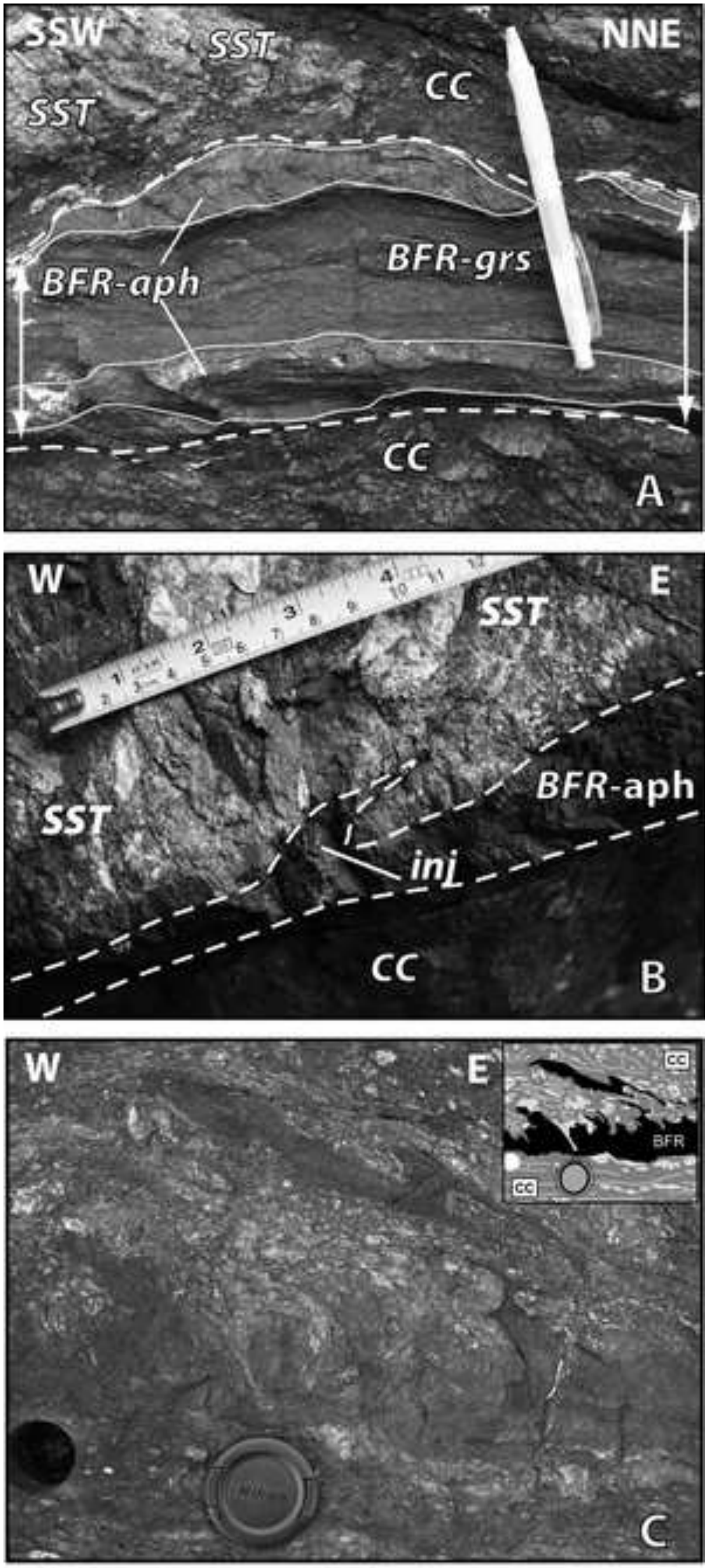

MENEGHINI ET AL. - FIGURE 5

Figure 6
Click here to download high resolution image

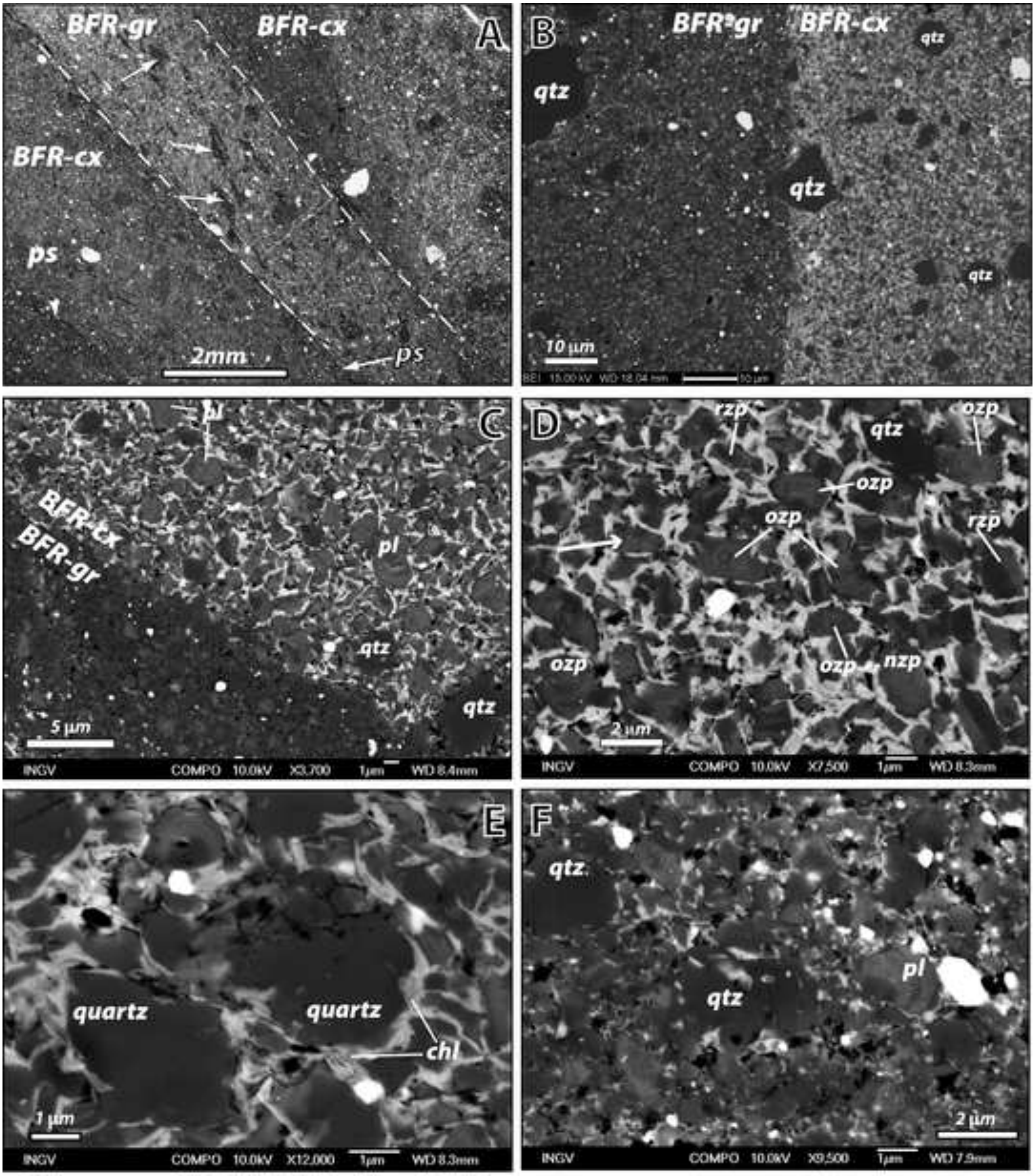

MENEGHINI ET AL. - FIGURE 6

Figure 7
Click here to download high resolution image

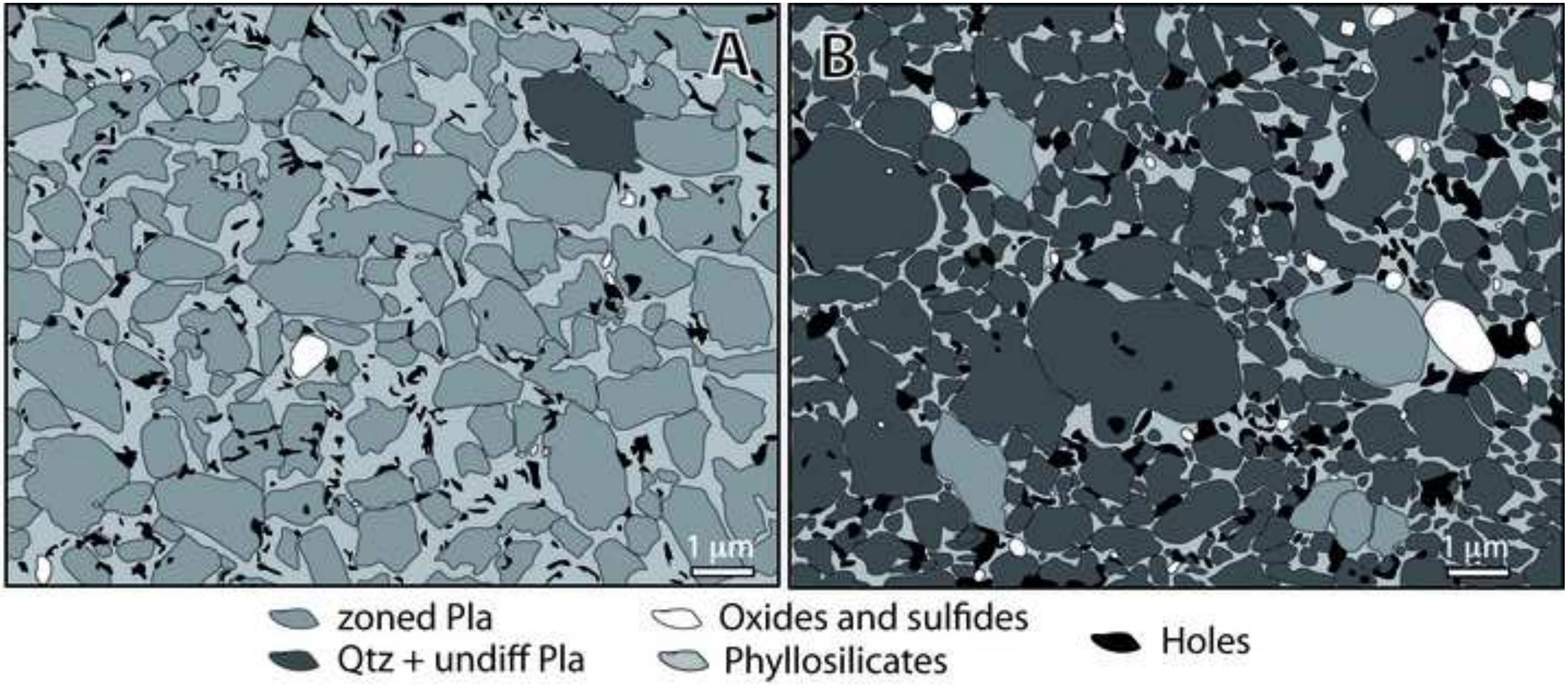

MENEGHINI ET AL. - FIGURE 7

Figure 8
Click here to download high resolution image

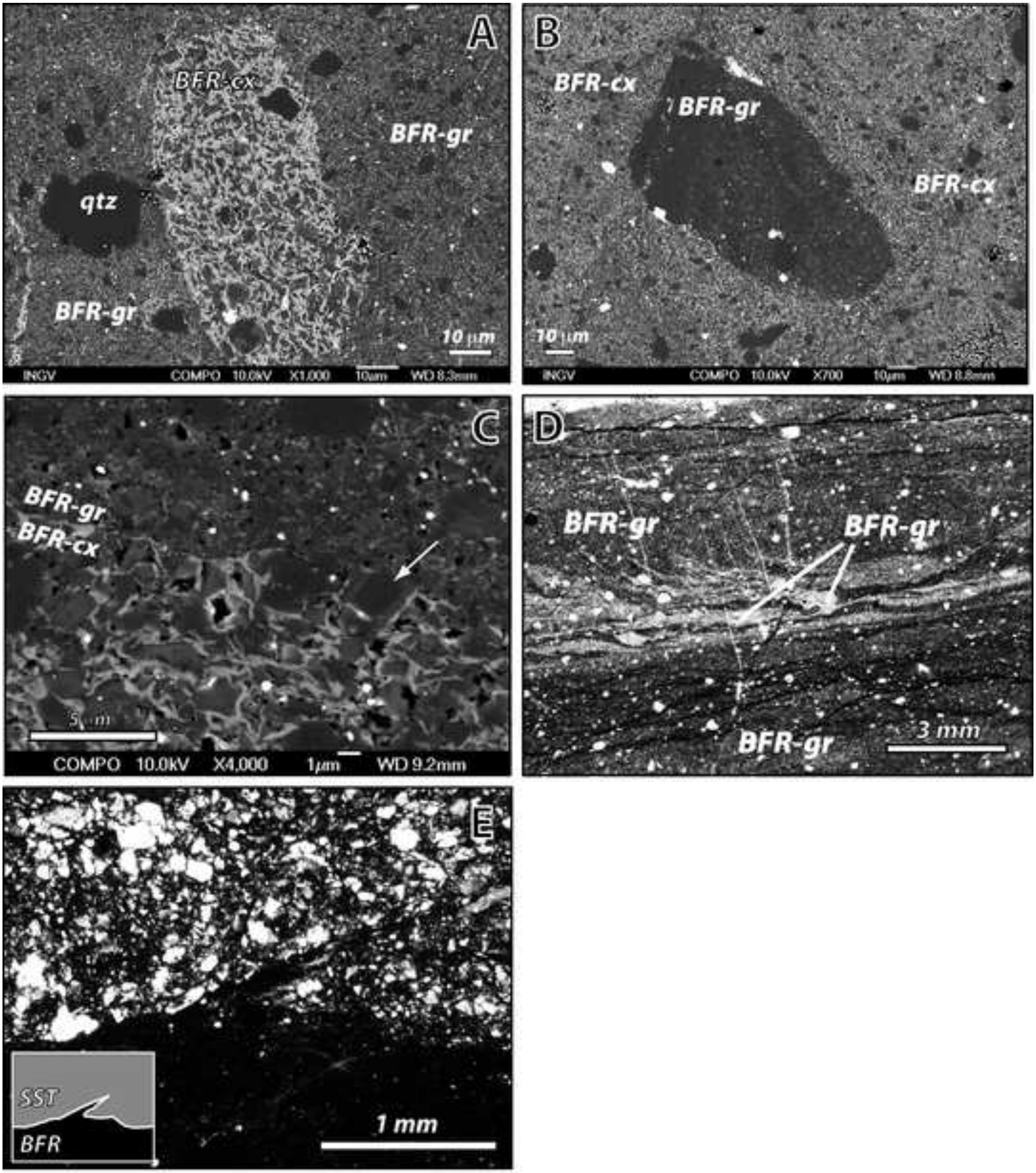

MENEGHINI ET AL. - FIGURE 8

Figure 9
Click here to download high resolution image

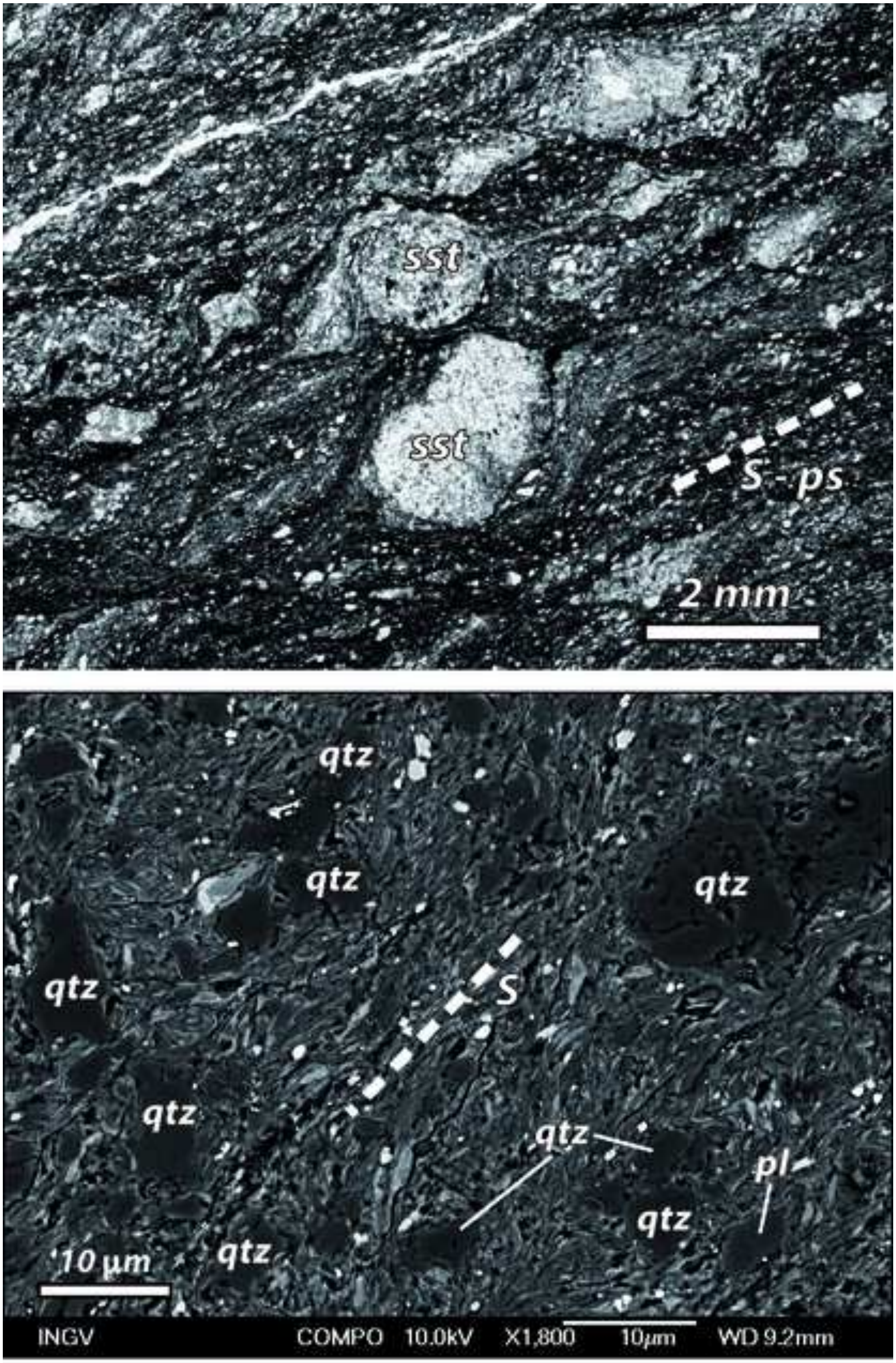

MENEGHINI ET AL. - FIGURE 9

Figure 10
Click here to download high resolution image

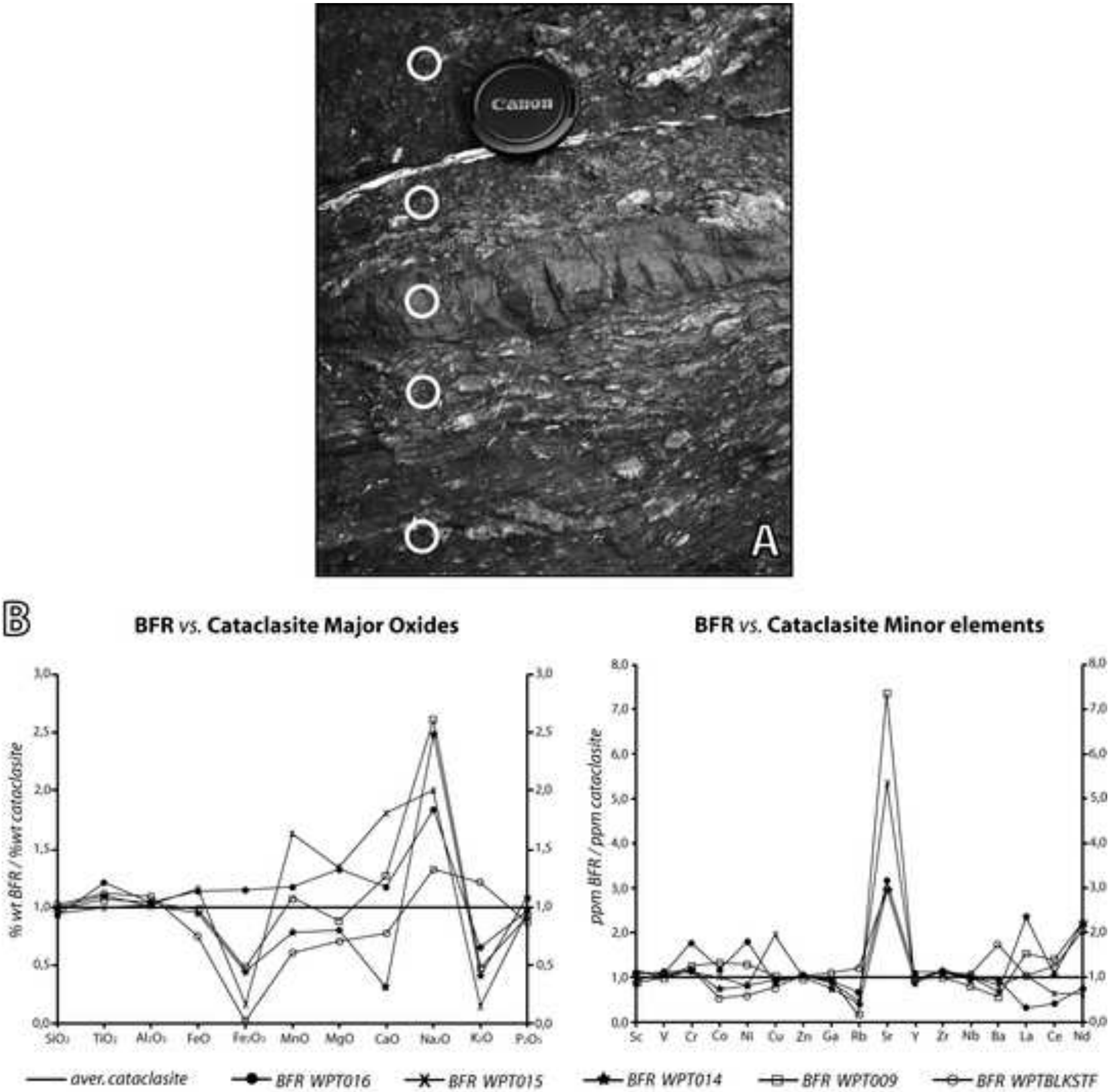

MENEGHINI ET AL. - FIGURE 10

Figure 11
Click here to download high resolution image

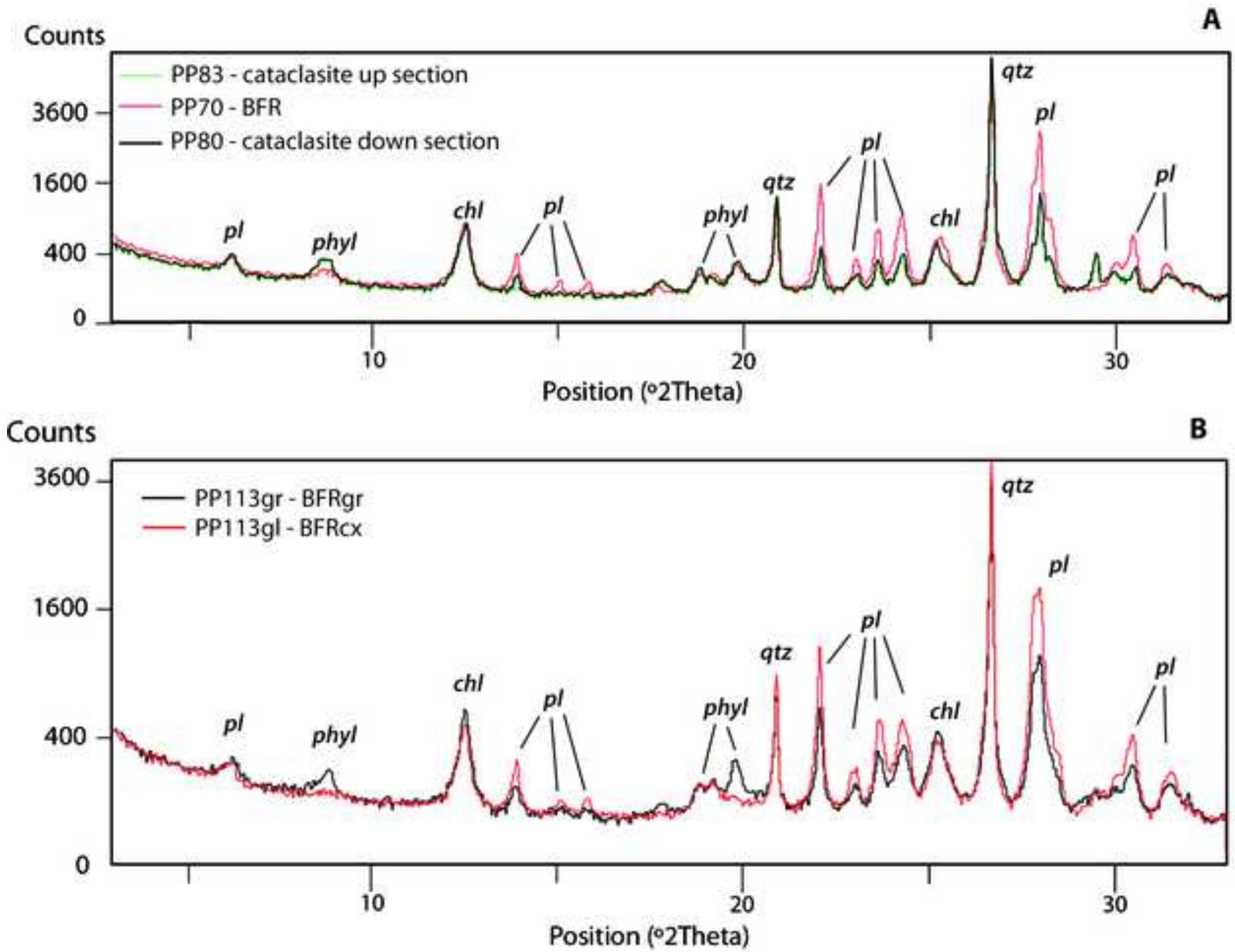

MENEGHINI ET AL. - FIGURE 11

Figure 12
Click here to download high resolution image

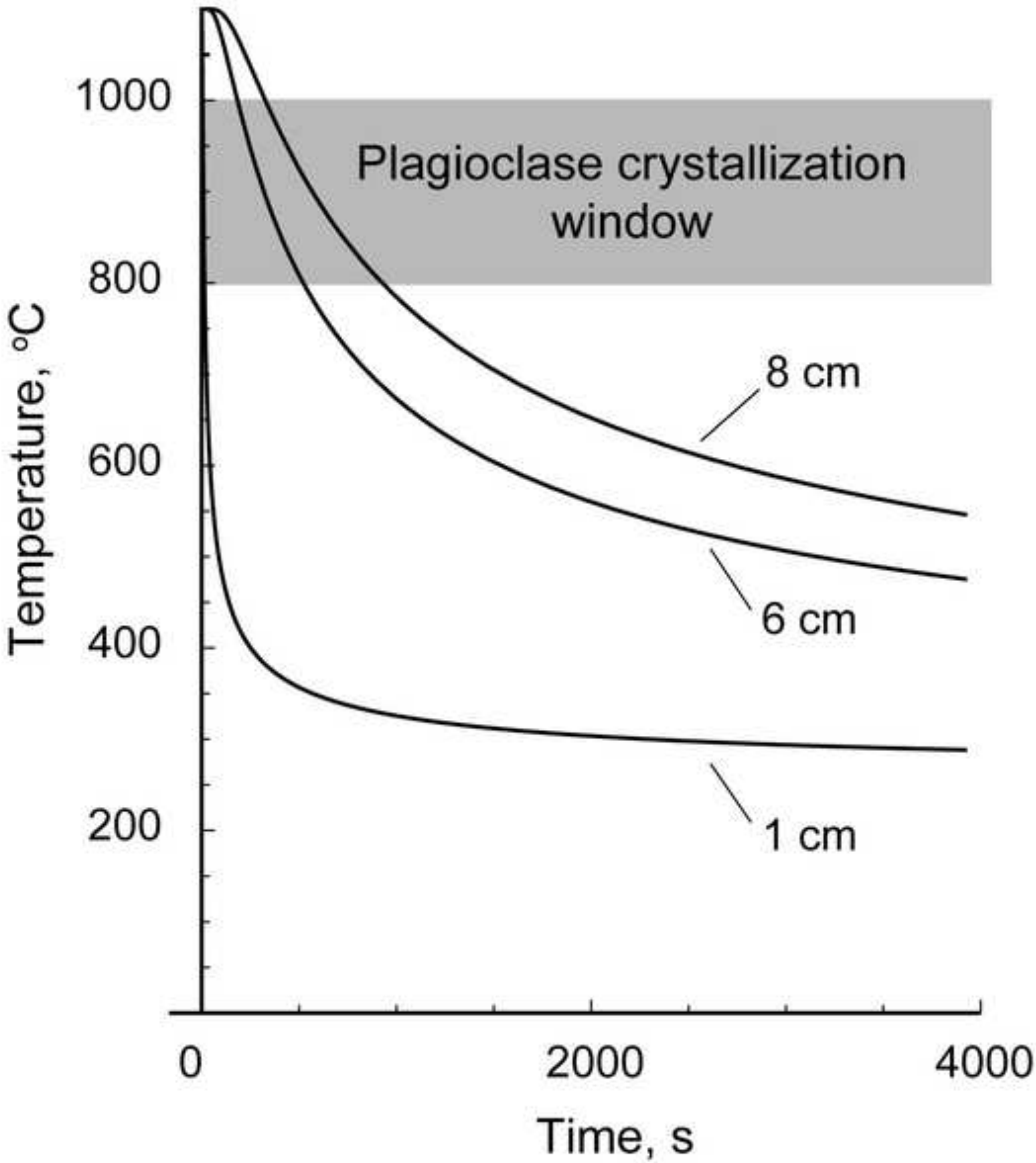

MENEGHINI ET AL. - FIGURE 11

Table

Sample	PP127	PP126fine	PP126coarse	(BFR-CC) Δ%	PP104a	PP104b	PP104c	(BFR-CC) Δ%	PP80	PP77	PP83	(BFR-CC) Δ%	PP97	PP98	(BFR-CC) Δ%	PP143	PP144	PP145	(BFR-CC) Δ%
Rock type	BFR	Cataclasite (fine grained)	Cataclasite (coarse grained)		Sandstone	BFR	Cataclasite		Cataclasite	BFR	Cataclasite		BFR	Cataclasite		gs-rich mélange	BFR	Cataclasite	
Position respect to BFR		0 cm downsection	3 cm downsection		0 cm upsection		0 cm downsection		10 cm downsection		10 cm upsection			< 10 cm downsection		0 cm upsection		0 cm downsection	
GPS locality	*WPT016*	*WPT016*	*WPT016*	*WPT016*	*WPT015*	*WPT015*	*WPT015*	*WPT015*	*WPT014*	*WPT014*	*WPT014*	*WPT014*	*WPT 009*	*WPT 009*	*WPT 009*	*WPTBLKSTF*	*WPTBLKSTF*	*WPTBLKSTF*	*WPTBLKSTF*
SiO_2	56,59	58,50	60,73	-5,1	70,84	58,03	58,81	-10,5	59,68	59,85	57,47	2,2	56,91	59,56	-4,4	59,03	61,26	58,82	4,1
TiO_2	0,99	0,83	0,79	22,4	0,51	0,94	0,86	37,2	0,80	0,93	0,86	11,5	0,87	0,87	0,7	0,82	0,95	0,84	13,7
Al_2O_3	17,25	16,52	16,19	5,5	12,94	18,16	17,26	20,3	16,01	17,35	17,69	2,9	17,51	16,96	3,3	16,10	18,73	16,84	11,3
FeO	7,58	7,09	6,10	14,9	3,35	6,77	6,74	34,2	6,32	6,69	7,40	-2,5	8,06	6,89	17,0	6,13	4,46	5,86	-23,9
Fe_2O_3	0,59	0,55	0,47	15,7	0,26	0,21	0,44	-40,0	0,39	0,11	0,09	-54,2	0,04	0,25	-84,0	0,37	0,05	1,88	-97,3
MnO	0,25	0,28	0,13	18,5	0,09	0,12	0,11	23,3	0,13	0,11	0,13	-20,1	0,17	0,10	64,7	0,16	0,08	0,12	-37,7
MgO	3,70	3,03	2,49	34,1	1,96	2,54	2,85	5,6	2,61	2,27	2,95	-18,2	3,69	2,74	35,0	4,25	1,98	2,75	-27,9
CaO	2,16	1,85	1,82	18,0	1,53	1,30	1,01	2,3	2,37	0,60	1,48	-68,7	2,18	1,20	82,3	3,37	0,86	1,08	-20,8
Na_2O	3,05	1,68	1,61	85,5	3,55	4,32	1,63	66,6	2,35	5,32	1,86	153,0	4,33	2,14	102,2	3,99	3,03	2,25	34,6
K_2O	1,84	2,75	2,87	-34,5	1,79	1,44	3,02	-40,0	2,45	1,17	2,99	-57,1	0,40	2,60	-84,7	0,34	3,14	2,54	23,3
P_2O_5	0,22	0,24	0,21	-1,9	0,13	0,27	0,28	30,3	0,22	0,25	0,24	10,2	0,25	0,25	-3,1	0,18	0,27	0,30	-11,5
L.O.I.	*5,61*	*5,86*	*5,78*	*-3,6*	*2,66*	*5,03*	*6,09*	*15,0*	*6,13*	*4,42*	*5,98*	*-27,0*	*5,03*	*5,67*	*-11,3*	*4,94*	*4,67*	*5,78*	*-19,2*
Tot	99,83	99,17	99,18		99,60	99,13	99,11		99,45	99,07	99,14		99,45	99,23		99,68	99,48	99,07	
Sc	22	20	20	11,5	17	21	23	6,7	19	23	22	11,7	20	22	-11,3	18	25	22	12,4
V	207	207	182	6,5	88	206	194	45,8	176	198	210	2,6	190	193	-1,1	158	214	191	12,1
Cr	181	102	102	77,1	60	125	113	44,6	98	122	111	16,3	133	106	25,2	204	132	115	15,0
Co	27	23	23	17,7	97	25	25	-59,5	35	20	20	-26,3	34	25	32,0	37	15	29	-47,5
Ni	92	58	45	79,2	24	45	55	14,4	46	40	51	-17,5	63	49	28,8	111	34	58	-41,7
Cu	59	77	60	-14,4	8	79	40	223,9	52	44	43	-6,3	73	70	3,2	57	56	72	-22,4
Zn	107	109	97	3,4	51	103	107	30,5	94	106	110	3,7	96	99	-2,3	83	108	103	5,4
Ga	17	19	18	-10,5	<5	16	19		15	13	20	-24,1	18	18	-4,0	15	20	18	9,0
Rb	54	84	85	-35,7	42	40	89	-38,7	72	32	87	-60,2	11	80	-85,6	8	95	79	20,3
Sr	368	121	115	212,5	315	553	103	164,1	121	317	96	191,5	926	126	637,3	616	386	130	197,4
Y	29	26	27	8,5	14	28	28	33,2	29	24	28	-14,0	26	27	-3,2	24	28	28	0,1
Zr	151	128	149	9,3	107	171	159	28,6	149	174	152	15,7	153	151	1,4	127	169	152	11,5
Nb	11	11	13	-4,5	10	13	14	16,5	12	13	13	6,3	11	13	-19,3	10	13	12	6,0
Ba	658	686	717	-6,3	1071	799	995	-22,7	778	593	943	-31,1	519	906	-42,7	649	1690	972	73,8
La	13	60	32	-70,8	<10	17	16		<10	37	16		29	19	52,5	25	36	35	4,5
Ce	25	73	53	-60,7	24	15	24	-37,3	36	41	41	5,3	41	30	37,6	28	38	31	23,3
Nd	27	42	33	-27,6	<10	21	33		16	35	16	120,3	33	15	120,5	13	39	19	104,4
Pb	<5	5	<5		<5	<5	<5		<5	<5	<5		<5	<5		<5	<5	<5	
Th	5	6	5	-14,5	5	4	6	-34,1	5	7	6	21,3	<3	6		<3	6	4	48,3
U	<3	<3	3		<3	<3	<3		5	4	3	6,3	3	5	-31,6	<3	3	4	-22,9

Table 2

	Average CC	CC standard deviation	Average BFR	BFR standard deviation
SiO_2	59,08	1,03	58,53	1,99
TiO_2	0,84	0,03	0,94	0,04
Al_2O_3	16,78	0,59	17,80	0,63
FeO	6,63	0,56	6,71	1,38
Fe_2O_3	0,58	0,59	0,20	0,23
MnO	0,15	0,06	0,14	0,07
MgO	2,77	0,19	2,84	0,81
CaO	1,54	0,49	1,42	0,73
Na_2O	1,93	0,31	4,01	0,98
K_2O	2,75	0,22	1,60	1,01
P_2O_5	0,25	0,03	0,25	0,02
L.O.I.	*5,90*	*0,17*	*4,95*	*0,45*
Tot				
Sc	21,32	1,55	22,32	1,92
V	193,23	12,47	203,05	9,05
Cr	106,86	6,35	138,58	23,97
Co	25,86	5,12	24,24	6,92
Ni	51,59	5,25	54,70	23,59
Cu	59,13	14,54	61,95	13,73
Zn	102,68	6,26	104,08	4,68
Ga	18,14	1,52	16,71	2,41
Rb	81,99	5,81	46,39	31,13
Sr	115,92	12,14	509,08*(406)*	249,11(*102,21)*
Y	27,46	0,95	26,91	1,77
Zr	148,53	9,49	163,74	10,60
Nb	12,52	1,00	12,30	1,19
Ba	856,77	127,40	851,70	479,81
La	29,63	16,85	26,57	11,01
Ce	41,22	16,84	31,94	11,59
Nd	24,76	10,83	30,89	7,20
Pb	5,08			
Th	5,37	0,73	5,21	1,44
U	4,14	1,06	3,65	0,75